

Human serum albumin–amlodipine binding studied by multi-spectroscopic, zeta-potential, and molecular modeling techniques

Parvin Atarodi Shahri¹ · Atena Sharifi Rad² · Sima Beigoli³ · Mohammad Reza Saberi⁴ · Jamshidkhan Chamani¹

Received: 8 April 2017 / Accepted: 27 October 2017 / Published online: 4 November 2017
© Iranian Chemical Society 2017

Abstract The fluorogenic property of amlodipine (AML) was for the first time exploited at various pH conditions to analyze the interaction with human serum albumin (HSA) as a probe. The techniques employed included fluorescence spectroscopy, zeta-potential measurements, polydispersion index (PDI) determination, three-dimensional fluorescence spectroscopy, circular dichroism (CD), and molecular modeling. The fluorescence of HSA was remarkably quenched by AML, and the quenching mechanism was considered as static through formation of a complex in the pH range of 5.4–9.4. The association constants and the number of binding sites were calculated at varying pH which implies that there was two set of binding site for AML upon HSA molecule. The obtained results display that there were more binding affinity between AML with HSA at pH = 7.4 and 8.4, whereas the least affinity was observed at pH = 9.4. The HSA–AML binding distances were determined to be shorter than 8 nm at the different pH, suggesting that energy transfer from HSA to AML may occur and HSA–AML complex was formed. Zeta-potential and resonance light scattering spectra results showed that the interaction between AML with HSA demonstrated different behaviors at the various pH such that

with an increasing pH, the C_{CIAC} (critical induced aggregation concentration) was decreased. In addition, the PDI values illustrated that pH effects caused differences in heterogeneity. According to CD data, the secondary structure contents of HSA upon interaction with AML were found to depend on pH, and an HSA–AML complex was clearly seen. Furthermore, the molecular modeling study indicated that AML was linked differently depending on the pH; for example, at pH 7.4, the bond between AML and HSA existed in site IIB and IIIA, and Trp214 was at a distance of 1.8 and 3.05 nm relative to AML, which was in agreement with the experimental analysis.

Keywords HSA · Amlodipine · Fluorescence spectroscopy · Circular dichroism · Zeta-potential · Molecular modeling

Introduction

A full understanding of the modes of drug actions requires the study of their interactions with all possible biological targets, including nucleic acids, enzymes, and proteins [1]. The binding form of a drug with serum albumin is the storage form for the drug [2]. Human serum albumin (HSA) is the most important and abundant constituent of blood plasma with a concentration of 42 g/L [3]. HSA is a globular protein with 66 kDa which is largely α -helical. It consists of a single polypeptide chain of 585 amino acid residues and is considered to have three specific domains (I, II, and III) for high-affinity binding of drugs that assemble to form a heart-shaped molecule with sides of 8 nm and a thickness of 3 nm. The tip of this heart shape is positively charged at

✉ Jamshidkhan Chamani
chamani.j@ut.ac.ir; chamani_j@yahoo.com

¹ Department of Biology, Faculty of Sciences, Mashhad Branch, Islamic Azad University, Mashhad, Iran

² Department of Chemistry, Faculty of Sciences, Neyshabour Branch, Islamic Azad University, Neyshabour, Iran

³ Endoscopic and Minimally Invasive Surgery Research Center, Mashhad University of Medical Sciences, Mashhad, Iran

⁴ Department of Medical Chemistry, School of Pharmacy, Mashhad University of Medical Sciences, Mashhad, Iran

physiological pH, and each of the sites consists of two sub-domains (A and B) and is stabilized by 17 disulfide bridges [4].

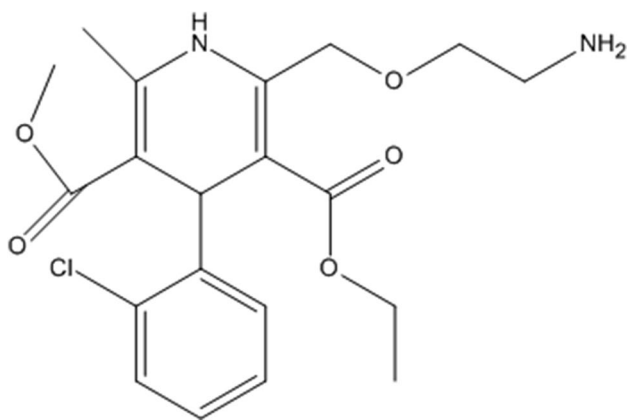
HSA constitutes up to 60% of the total protein amount and contributes to 80% of the colloid osmotic blood pressure. Moreover, it is chiefly responsible for the maintenance of blood pH [5]. In blood plasma, the exceptional ability of HSA is its capacity to bind a diverse variety of ligands (often more than 94% of the drug is attached to the protein), due to the presence of two principal binding sites (i.e., Sudlow's site I and site II) which Site I is dominated by strong hydrophobic interaction with most neutral, bulky, heterocyclic compounds, while site II mainly sees dipole–dipole, van der Waals, and/or hydrogen bonding interactions with many aromatic carboxylic acids [6]. Ligands may include fatty acids, hormones, bilirubin, drugs, and a large diversity of metabolites with dissociation binding constants in the range of 10^{-3} to 10^{-8} mol L⁻¹ [7].

Amlodipine (AML), R, S-2 [(2-aminoethoxy) methyl]-4-(2-chlorophenyl)-ethoxycarbonyl-5-methoxycarbonyl-6-methyl-1,4-dihydropyridine (Scheme 1), is a potent calcium channel blocker used in the treatment of hypertension and angina pectoris [8]. These blockers, also known as calcium antagonists, like other calcium channel blockers, inhibit calcium influx into cardiac and vascular smooth muscle cells, via L-type “voltage-gated” calcium channels, leading to dilatation of both arteries and arterioles and causing an inhibition of: (1) sinoatrial pacemaker activity and atrioventricular conduction, (2) cardiac inotropy, and (3) vascular contraction [9]. More recent studies show that amlodipine besylate and other blockers of calcium channels inhibit tumor proliferation by hampering the incoming flow of calcium ions causing the destruction of internal reservoirs of calcium ions in cancer cells [10]. Amlodipine is available alone and in combination with benazepril or atorvastatin. AML has a 24-h duration of action, permitting once-daily dosing [11]. Like all

antihypertensives from the 1,4-dihydropyridine group, amlodipine besylate is degraded under the influence of light, causing the 1,4-dihydropyridine ring to convert into a pyridine ring. The resulting pyridine derivative of AML causes the loss of pharmacological activity and also exhibits some toxicity. It is also a potential cause of cancer [12].

Protein–ligand interactions play an important role in a variety of biological processes. It is thus important to study the interaction of the AML with HSA since HSA–AML binding is essential in pharmacology and pharmacodynamics [2]. The affinity of binding between ligand and HSA can dominate its distribution in target tissues, affect its elimination from the body, and influence its therapeutic/toxicological effects. Also, it is generally believed that the binding of ligands to albumin can conspicuously alter their overall activity profile, including distribution, transportation, excretion, and toxicity, which is correlated with their affinities toward serum albumin [5]. Furthermore, the therapeutic drug effect is related to the balance between the bound and unbound fraction of the drug. To characterize these interactions at the molecular level, optical techniques have become valuable tools since these methods are sensitive and relatively easy to use. Also, they can be employed to shed some light on how the probe binds under different solvent conditions and in particular when pH is varied [3].

The objective of this work was to determine the binding affinity and binding site of AML to HSA and to evaluate and compare the binding property between AML and HSA in various pH. By measuring the intrinsic fluorescence quenching of HSA, the accessibility of AML to the fluorophore groups of HSA can be estimated [13]. The fluorescence method is based on the fact that the Trp residues in proteins have intrinsic fluorescence. The spectral changes observed upon the binding of ligand with fluorophores of proteins are important for the investigations of the topology of binding sites, conformational changes and characterization of substrate to AML binding. Also synchronous fluorescence spectroscopy is used to monitor the changes of protein structure and conformation. Unlike conventional fluorescence excitation and emission spectroscopy, synchronous fluorescence spectroscopy is taken as a combined function of excitation and emission wavelength [14]. The aim was also to analyze the effect of different pH in secondary structure alterations of HSA in the presence of AML. Here, the interaction between HSA and AML was investigated at different pH by different methods. Moreover, the molecular modeling is employed to determine the binding site of AML on HSA at varying conditions in order to demonstrate the various behaviors of the interaction between HSA and AML.



Scheme 1 Chemical structure of amlodipine besylate

Experimental

Materials and solutions

HSA and AML were purchased from Sigma Chemical Co. and used without further purification. An HSA (4.59×10^{-5} mM) stock solution was prepared in phosphate buffer, and a stock solution of AML (0.002 mM) was also prepared in phosphate buffer but at varying pH.

Apparatuses

Fluorescence measurements

Fluorescence spectra were recorded on an F-2500 spectrofluorometer (Hitachi, Japan) linked to a personal computer and equipped with a 150-W xenon arc lamp, gating excitation and emission monochromators, and a Hitachi Recorder. Slit widths for both monochromators were set at 5 nm. A 3-cm quartz cell was used. A Metrohm digital pH meter (Metrohm, Germany) was utilized for the pH adjustment, which was calibrated by two points. Fluorescence intensities were corrected for inner filter and dilution effects before analysis of the binding and quenching data. Also, we used derivative fluorescence spectroscopy for the detection of transitions in the environment of amino acids with a phenyl ring (i.e., aromatic amino acids). Furthermore, the fluorescence intensities were corrected for absorption of excitation light and reabsorption of emitted light to decrease the inner filter and dilution effects using the formula:

$$F_{\text{cor}} = F_{\text{obs}} e^{(A_{\text{ex}} + A_{\text{em}})/2}, \quad (1)$$

where F_{cor} and F_{obs} are the fluorescence intensities corrected and observed, A_{ex} and A_{em} are the absorption of the system at excitation and emission wavelength, respectively [15].

Resonance light scattering (RLS)

RLS spectra were recorded with an F-2500 fluorescence spectrophotometer (Hitachi, Japan) by simultaneously scanning the excitation and emission spectra from 280 to 600 nm with $\Delta\lambda = 0$ nm, $\Delta I_{\text{RLS}} = I_{\text{RLS}} - I_{\text{RLS}}^0$, where I_{RLS} and I_{RLS}^0 were the intensities of the system with and without AML, respectively. The slit width was set at 5.0 nm. The RLS technique is based on the long-range assembly of probe molecules on the surface of the protein, which result in an enhanced RLS intensity. This has proven to be useful in the investigation of aggregations of small molecules.

Synchronous fluorescence spectroscopy

The synchronous fluorescence spectroscopy serves as a robust method for quantitative determination in a single

measurement. Such synchronous fluorescence spectra gives only characteristic information for the Tyr and Trp residues of HSA when the wavelength interval ($\Delta\lambda = \lambda_{\text{em}} - \lambda_{\text{ex}}$) is 15 nm and 60 nm, respectively.

Three-dimensional fluorescence spectroscopy

Three-dimensional fluorescence spectroscopy was performed on an FP-2600 fluorescence spectrophotometer (Jasco, Japan) under the following conditions: The emission wavelength was recorded between 220 and 500 nm, the initial excitation wavelength was set to 220 nm and increased with increments of 5 nm, and the number of scanned curves and other scanning parameters was identical to those of the fluorescence emission spectroscopy. Three-dimensional fluorescence spectroscopy greatly enhances the selectivity of fluorescence spectra.

UV–visible spectroscopy

The UV–visible spectra were collected at room temperature on a double-beam V-630 spectrophotometer (Jasco, Japan) in 1-cm quartz cells. The slit width was set to 5 nm, and the wavelength range was 200–500 nm.

Circular dichroism spectroscopy (CD)

Far UV-CD experiments were carried out on a Jasco-815 spectropolarimeter (Jasco, Japan) equipped with a Jasco 2-syringe titrator under constant nitrogen flush at room temperature. The instrument was controlled by Jasco's Spectra Manager TM software, and the scanning rate, bandwidth, and response were set as 50 nm min^{-1} , 1 nm, and 2 s, respectively. The instrument was calibrated by d-10-camphorsulfonic acid. A quartz cuvette with a pathlength of 1 mm was used, and each spectrum was the average of five successive scans (with the protein concentration held constant). The samples for CD were prepared with a fixed concentration of HSA (4.59×10^{-5} mM) and a varied drug concentration while maintaining equal volumes. The induced ellipticity was obtained as the ellipticity of the HSA–drug mixtures after subtraction of that of the drug at the same wavelength. It is expressed in degrees. The results are given as the mean residue ellipticity [θ], defined as:

$$[\theta] = 100 \times \theta_{\text{obsd}} / (LC), \quad (2)$$

where [θ] is the observed ellipticity in $\text{deg cm}^2 \text{ dmol}^{-1}$, θ is the observed ellipticity at a given wavelength in deg, C is the concentration in residue mol cm^{-3} , and L is the length of the light path in the cell [16].

α -helix contents were also calculated from the molar ellipticity derived from Eq. [3] according to

$$\% \alpha - \text{helix} = ([\theta]_{222} + 3000) / 39000. \quad (3)$$

Zeta-potential

The electrostatic interaction of HSA–AML can be controlled by varying their surface charges and can be determined by measuring the zeta-potential of these particles. The zeta-potential can be altered by changing the pH, conductivity, or concentration of a formulation component. Zeta-potential values were calculated from the electrophoretic motilities, in μE , using Henry equation [17]:

$$\zeta = 3\mu E\eta / 2\varepsilon_0\varepsilon_r \times 1/f(\kappa\alpha), \quad (4)$$

where ε_0 is the permittivity of vacuum, ε_r and η are the relative permittivity and viscosity of water respectively, α is the particle radius, and κ the Debye length. The function $f(\kappa\alpha)$ depends on the particle shape, and for our system it was determined for $\kappa\alpha > 1.14$ as

$$f(\kappa\alpha) = 3/2 - 9/2\kappa\alpha + 75/\kappa^2\alpha^2, \quad (5)$$

where κ is the reciprocal Debye length.

The polydispersity index (PDI) is an indication of the particle size distribution. The zeta-potential and size measurements were performed using a Zetasizer, Nano Series—ZS (Malvern Instruments Ltd, UK).

Principles and calculations of molecular modeling

Molecular modeling is obtained by the technique of molecule docking computing in which ligands are located to the active site of the corresponding receptor after which the interaction is evaluated and the most possible modeling is deduced according to the principles of the lowest energy combined with geometrically matching the quality between ligand and receptor. The crystal structure of HSA titled 1AO6 was taken from the Brookhaven Protein Data Bank (<https://www.rcsb.org/pdb>). The 3D structure of AML was obtained from the ChemBio Office 2007 software, whereas a minimization of AML was done with the AM1 method, semi-empirically, in HyperChem7 and then entered in AutoDock 4. To reach the most stable form of protein minimization, two steps were performed: (1) The MOE software was used for the protein at different pH conditions; In protonate 3D menu temperature was set as 300 K, while the pH was changed as reported. (2) The HyperChem program (version 8.0.9-RECOiL) was used to merge files that consisted of drug and protein. Semi-empirical method was set for the minimization using AM1 algorithm. In HyperChem geometry, optimization Polak–Ribiere algorithm was set, and the RMS gradient was set 0.01 kcal/mol to terminate the minimization cycles.

AutoDock 4 was employed to perform docking calculations (<https://www.scripps.edu/pub/olson-web/doc/autodock/>) on a Slax Linux platform. Lamarckian genetic

algorithm (LGA) implemented in AutoDock was applied to calculate the possible conformation of the drug that binds to the protein. Whole the protein was considered in the grid box, and then grid maps were generated with 1-Å spacing by the autogrid program for the whole protein in order to detect the docking grid and active sites. Each docking experiment was derived from 100 different runs while the population size was set to 150. Flexible backbone and side-chain option were not utilized in this study. The best docking results were selected based on their K_i value that was correlated to their δG energy. SPDBV, Molegro Molecular Viewer, and ViewerLite were utilized to perform the protein analysis and graphics outputs. As the pH affects the secondary structure of the protein, we applied the SPDBV software to track the conformational changes in the secondary structure level of the protein before and after minimization at the different pH values. All atoms were taken into account due to the similarity of proteins. (The proteins were basically the same except for different folding due to altered the value of pH.) Furthermore, the binding site of the protein was detected using the multiple alignment technique. The sequence of HSA was taken from Uniprot (code: P02768). Multiple alignments were also done using conserved, semi-conserved, and far proteins of HSA. The active site was predicted using two sites: <https://medock.csnie.ntu.edu.tw> and <https://www.sbg.bio.ic.ac.uk/~3dligandsite/>.

Procedures

HSA and AML were dissolved in 50 mM phosphate buffer pH = 7 and diluted to 0.05 and 0.002 mM, respectively, corresponding to low usage dose concentrations. The interaction time was investigated, and the results showed that 3 min was enough for the stabilization. The fluorescence spectra were then measured. (The excitation wavelengths were 280 and 295 nm, and the emission wavelengths were 290–600 nm.) The zeta-potential results and UV absorbance spectra of AML and HSA were recorded, and spectral scanning curves were obtained under the same conditions. All experiments were applied in the pH range of 5.4–9.4.

Results and discussion

Fluorescence quenching measurement of the HSA–AML complex

Qualitative analysis of binding of a chemical compound to HSA, i.e., the location of the AML binding site and the changes in the environment around Trp 214, can be precisely obtained by using a fluorescence technique [13]. Fluorescence of HSA originates from Trp, Tyr, and Phe residues. A single Trp residue, Trp 214, located in the depth of

sub-domain IIA of HSA, is largely responsible for the intrinsic fluorescence of HSA. This is due to the quantum yield of Phe being very low and the fluorescence of Tyr being almost totally quenched if it is ionized or near an amino group, a carboxyl group, or a Trp residue 2. This viewpoint was well supported by the experimental observations made by Sulkowska et al. [18].

Quenching is the result of various inter- and intramolecular interactions, such as excited-state reactions, energy transfer, ground state complex formation, and collisional quenching (dynamic quenching) [19]. Figure 1a–e shows the dependence of the HSA fluorescence with an increasing AML concentration in potassium phosphate buffer solutions in the pH range between 5.4 and 9.4 when the excitation wavelength was 280 nm. HSA has a fluorescence emission spectrum in the 300–400 nm wavelength range, with an emission maximum at 338–342 nm at the pH values in question. The result showed that in the pH range between 5.4 and 9.4 gradual decreases in the fluorescence intensity of HSA was occurred which was caused by quenching. The variations of HSA emission maximum at different pH are a reflection of the changes in local environment of Trp residues and consequently a change in structure of the HSA [20]. Therefore, the observed spectral shift was due to the alterations of polarity of the protein environment, since a similar blueshift was observed at all pHs, and the hydrophobicity was increased in the vicinity of the Trp residue when the concentration of AML was enhancement [21, 22].

An isoactinic point formed at pH = 8.4 and 9.4 indicated an equilibrium between the free AML and the HSA–AML complex. In other words, an isoemissive point was considered to be direct evidence of drug–protein complex formation [23]. Figure 1 shows that a complex was possibly formed between AML and HSA at all pH and that this complex was responsible for the quenching of the fluorescence of HSA. The Stern–Volmer equation is often applied to describe the fluorescence quenching [24]:

$$F_0 / F = 1 + kq\tau_0[Q] = 1 + KSV[Q]. \quad (6)$$

In Eq. [6], F_0 and F are the fluorescence intensities before and after addition of the quencher, respectively, KSV is the Stern–Volmer dynamic quenching constant, kq is the quenching rate constant of the biomolecule, τ_0 and $[Q]$ are the average lifetime of the biomolecule and concentration of the quencher, respectively. We then have:

$$KSV = kq \tau_0. \quad (7)$$

The average lifetime of the molecule's fluorescence as around 10^{-8} s [25], an approximate quenching constant (kq , $L \text{ mol}^{-1} \text{ s}$) could be obtained according to Eq. [7]. Since the maximum scatter collision quenching constant of individual quenchers with a biopolymer (kq) is $2.0 \times 10^{10} L \text{ mol}^{-1} \text{ s}^{-1}$, the quenching rate of the biomolecule by a quencher being

larger than this value demonstrates that quenching was not dynamic and that a protein–drug complex was formed [26].

The value of kq for interaction between AML with HSA in the pH range between 5.4 and 9.4 was calculated and is listed in Table 1 when $\lambda_{ex} = 280$ nm. The obtained results demonstrated that the value of kq for quenching of HSA with AML were greater than $2.0 \times 10^{10} L \text{ mol}^{-1} \text{ s}^{-1}$, and thus the static quenching is main quenching mechanism and AML–HSA complex was formed at all pH.

The fluorescence data were further studied by using the modified Stern–Volmer equation [26, 27]:

$$F_0 / (F_0 - F) = 1/fa + 1/Ka fa[Q], \quad (8)$$

where Ka is the effective quenching constant for the accessible fluorophores, which are analogous to associative binding constants for the quencher–acceptor system and fa is the fractional maximum fluorescence intensity of protein summed up.

The inset of Fig. 1a–e shows the modified Stern–Volmer plots for the HSA–AML system at different pH values at two excitation wavelengths of 280 and 295 nm. The modified Stern–Volmer plots at all pH showed two regressions curves when $\lambda_{ex} = 280$ nm which introduces the existence of more than one binding site with different binding affinity at high drug concentration for AML upon HSA, whereas the linear modified Stern–Volmer plot was observed at $\lambda_{ex} = 295$ nm which cleared that there is just a single class of binding site for AML upon HSA [28]. The values of fa for HSA–AML complex at various pH are summarized in Table 1 at $\lambda_{ex} = 280$. The fa_1 was greater than fa_2 at all pH, but when pH = 7.4, the value of $fa_2 > fa_1$ which implies that interaction with AML induced some structural changes in HSA and provide more accessible fluorophore for AML. When pH = 7.4, fa_1 was 1.12 (at all pH approximately $fa_1 = 1$), which meant that 100% of the fluorescence of Trp residues in HSA could be quenched [29].

Calculation of binding parameters

The 1:1 binding of a drug to a protein to form a complex can be described by the following equation, where $[D]$, $[P]$, and $[DP]$ are the free drug, free protein, and drug–protein complex concentrations, respectively [30]:



From the stoichiometric coefficient of Eq. [9], the total protein concentration can be written as:

$$[B] = [QnB] + [B]. \quad (10)$$

Furthermore, the resultant constant Ka is given by:

$$Ka = [Qn \dots B] / [Q]n [B]. \quad (11)$$

If the overall amount of biomolecules (bound or unbound with the quencher) is B_0 , then $[B_0] = [QnB] + [B]$, here $[B]$ is the concentration of unbound biomolecules; then the relationship between fluorescence intensity and the unbound

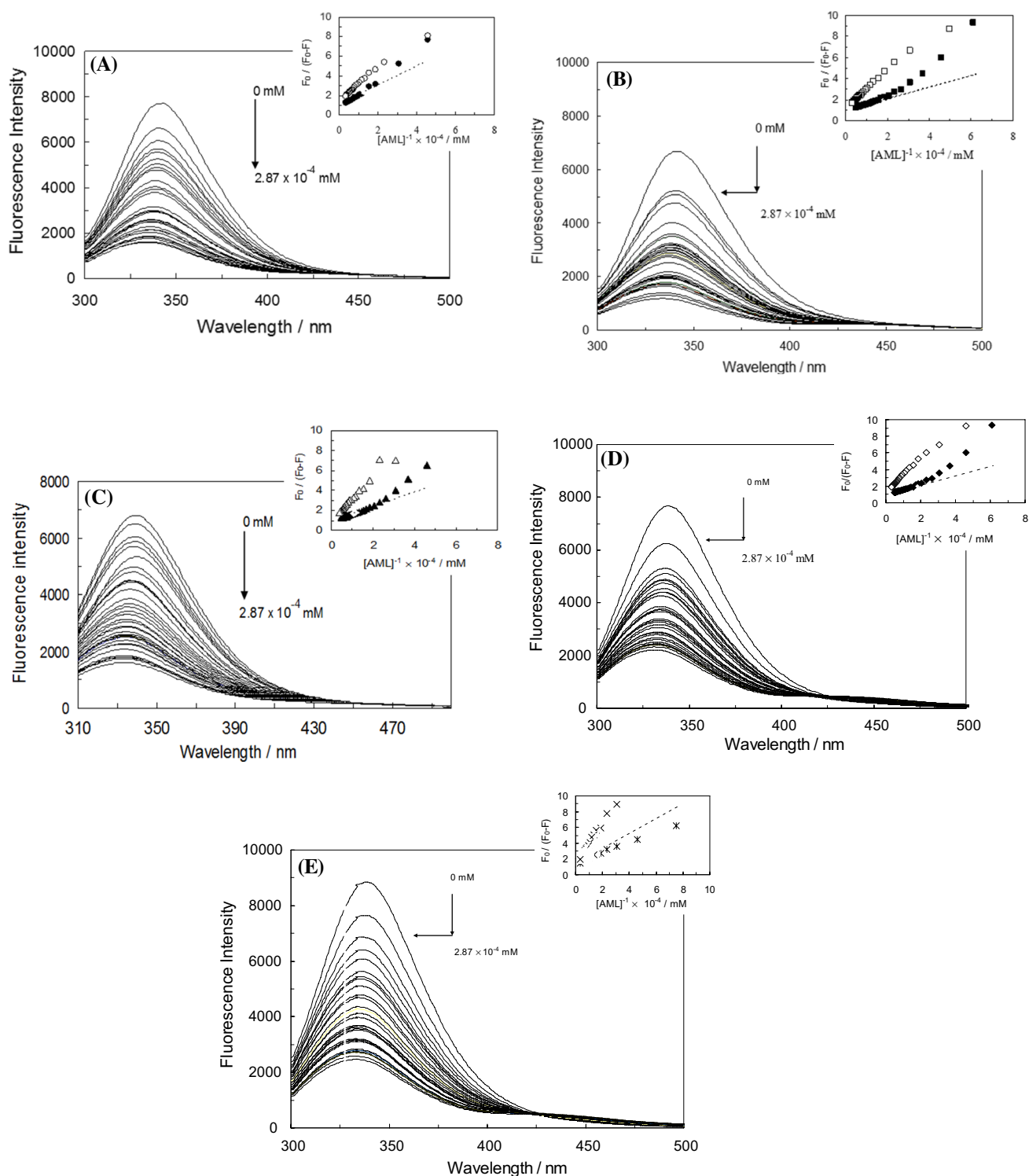


Fig. 1 Effect of AML on emission fluorescence spectra of HSA at **a** pH = 5.4, **b** pH = 6.4, **c** pH = 7.4, **d** pH = 8.4, **e** pH = 9.4. The concentration of HSA was 4.59×10^{-6} mM and that of AML was increased from 0 to 2.87×10^{-4} mM, T = 298 K; the fluorescence excitation was at 280 nm, the inset in each image indicates modi-

fied Stern–Volmer results at $\lambda = 280$ nm at pH = 5.4 (filled circle), 6.4 (filled square), 7.4 (filled triangle), 8.4 (filled diamond), 9.4 (∇), $\lambda = 295$ nm at pH = 5.4 (open circle), 6.4 (open square), 7.4 (open triangle), 8.4 (open diamond), 9.4 (\ast)

Table 1 Quenching rate constant of the biomolecule (k_q) and the fraction of accessible fluorophore (f_a) of the AML–HSA system at different pH; $T = 298\text{ K}$, $\lambda_{\text{ex}} = 280\text{ nm}$

pH	$k_{q1} \times 10^{-12}/\text{M}^{-1}$	$k_{q2} \times 10^{-12}/\text{M}^{-1}$	f_1	f_2	R_1^a	R_2^a
5.4	1.08 ± 0.03	1.41 ± 0.02	1.09	4.04	0.99	0.99
6.4	1.14 ± 0.01	1.24 ± 0.03	0.91	0.64	0.99	0.98
7.4	1.97 ± 0.02	2.03 ± 0.03	1.12	1.57	0.99	0.98
8.4	1.97 ± 0.03	2.18 ± 0.02	1.13	0.79	0.99	0.98
9.4	0.88 ± 0.03	0.86 ± 0.01	0.99	0.60	0.99	0.99

^a R is the correlation coefficient

biomolecule is given as $[B]/[B_0] = F/F_0$. On the other hand, for the static quenching procedure, the binding constant K and the number of binding sites n can be elicited from the following equation [31]:

$$\log(F_0 - F)/F = \log Kb + n \log [Q], \tag{12}$$

here $[Q]$ is the total concentration of quencher, n can be deduced from the slope of linear regressions of the curve $\log(F_0 - F)/F$ versus $\log[Q]$, and K is determined from the intercept of the linear regressions. In this study, the binding parameters for the HSA–AML system at various pH have been derived from fluorescence quenching data obtained at $\lambda_{\text{ex}} = 280\text{ nm}$. Table 2 shows the values of K_b and n , according to Eq. [12]. It is obvious that the binding constant at $\text{pH} = 7.4$ was remarkably larger than at other pH values and that lowest binding affinity is belong to HSA–AML complex at $\text{pH} = 9.4$. The calculated value of K_{b1} for binding of AML to HSA was greater than K_{b2} at $\text{pH} = 7.4$ and 8.4 which suggests that the HSA change conformational reduced the binding affinity of AML to HSA whereas at other pH values corresponding alteration provided more affinity between drug and protein ($K_{b2} > K_{b1}$). In addition, the more and less number of binding sites for HSA–AML complex was at $\text{pH} = 7.4$ and 9.4 , respectively. At all pH conditions, the number of binding site (n_1 and n_2) was approximately equal 1 which imply that about one molecule of AML bound to one class of site on HSA [32]. It can be deduced that AML was suitable for binding to the HSA molecule at $\text{pH} = 7.4$ and 8.4 . Therefore, since the physiological pH is 7.4 , another investigation was carried out at $\text{pH} = 7.4$.

Table 2 Binding constants, K_b , and the number of binding sites, n , at different pH of the HSA–AML complex; $T = 298\text{ K}$, $\lambda_{\text{ex}} = 280\text{ nm}$

pH	$K_{b1} \times 10^{-4}/\text{M}^{-1}$	$K_{b2} \times 10^{-4}/\text{M}^{-1}$	n_1	n_2	R_1	R_2
5.4	6.397	7.103	1.206	1.209	0.98	0.99
6.4	0.3329	1.4903	0.855	1.025	0.98	0.99
7.4	9336.84	9.9770	1.885	1.197	0.99	0.99
8.4	795.609	10.505	1.629	1.193	0.98	0.99
9.4	0.1265	0.8107	0.785	0.991	0.98	0.99

Second derivative fluorescence spectroscopy

The second derivative fluorescence spectroscopy is a sensitive and reliable technique for monitoring and characterizing the transitions that take place in the environment of aromatic amino acids, mainly Trp, in a protein [33]. The use of this technique has several advantages such as the technique is not dependent on the turbidity of the sample, which makes it unnecessary to correct for light scattering, and its selective excitation of Trp makes it much easier to separate effects due solely to these residues from those due to Trp and Tyr together, as occurs in absorption spectroscopy.

Figure 2a indicates the second derivative of interaction between AML with HSA at $\text{pH} = 7.4$, and several aspects of the typical second derivative fluorescence spectra are pointed out below. The most salient features common to these spectra were: a minimum peak at around $334\text{--}341\text{ nm}$, a relatively fixed maximum at $377\text{--}390\text{ nm}$, and a shoulder around $368\text{--}369\text{ nm}$. The origin of negative band was probably the transition of the electrons back to the different vibration levels of the ground state. The position and the intensity of the second derivative spectra were altered with a raise of the AML concentration. The spectra of the second derivative increased, and the observation of a blueshift signified effect of AML upon HSA structure and a decreased in the polarity around Trp214 residue. The H parameter depends on the dielectric constant of the solvent [34, 35], and it was used as an empirical measure of the effect of the relative hydrophobicity of the solvent on the second derivative spectra of HSA–AML complex and shown in Fig. 2b. As the AML concentration increased, the H factor decreased linearly in the whole pHs implying an increase in the polarity around the aromatic amino acid, mainly Trp, and the hydrophobicity reduced. These results express that AML–HSA complex

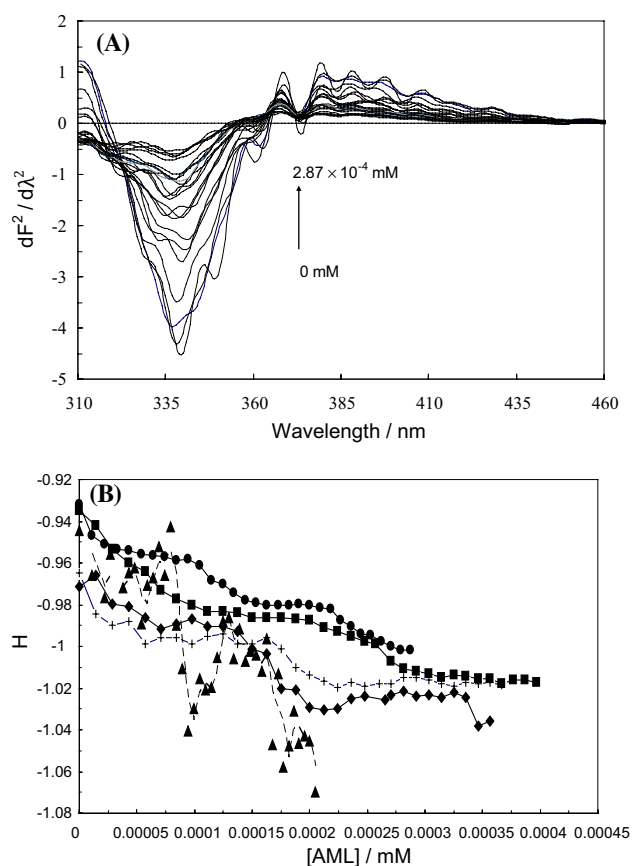


Fig. 2 **a** Second derivative fluorescence spectra for the AML–HSA complex at pH = 7.4, [HSA] = 4.59×10^{-6} mM and [AML] = 2.87×10^{-4} mM. **b** The slope of H versus the concentration of AML at pH = 5.4 (filled circle), 6.4 (filled square), 7.4 (filled triangle), 8.4 (filled diamond), 9.4 (∩) at 280 nm, T = 298 K

formation induced a looser structure of the protein and causing a further exposure of Trp residues from the core of HSA to the polar solvent. pH = 7.4 and pH = 5.4 agree with the sooner and the latest transfer of the Trp residue to less hydrophobic medium or exposure to the polar solvent.

Synchronous fluorescence spectroscopic studies of HSA

Synchronous fluorescence spectroscopic introduced by Lloyd and Evett, who initially applied it in the field of forensic science, and it has been used to investigation the microenvironment of amino acid residues by measuring the shift of emission maxima [36]. The main characteristics of synchronous fluorescence are a narrowing of the spectral band, a simplification of emission spectra, as well as a reduction and avoidance of different perturbing effects [37]. We have ascertained that it was the binding of AML to HSA that caused the fluorescence quenching of HSA, but it is still a puzzle whether the binding affects the conformation and/or microenvironment of HSA

[38]. According to Miller, a distinction of the difference between excitation wavelength and emission wavelength ($\lambda_{em} - \lambda_{ex}$) reflects the spectra of chromophores of various natures [39].

The selection of $\Delta\lambda$ in synchronous spectrofluorometry is very important. The influence of $\Delta\lambda$ can be substantial to the shape, location, and signal intensity of a fluorescence peak [40]. When the D values, ($\Delta\lambda$), between emission and excitation wavelength are set at 15 or 60 nm, the synchronous fluorescence can provide the characteristic information of Tyr or Trp residues in HSA, respectively, 13. Since the relationship of the synchronous fluorescence intensity (ISF) and the concentration of protein should follow the synchronous fluorescence intensity (SFI) equation, the SFI should be in direct proportion to the concentration of the protein [41]:

$$SFI = KcdE_{ex}(\lambda_{em})E_{em}(\lambda_{ex} + \Delta\lambda), \quad (13)$$

here SFI is the relative intensity of synchronous fluorescence, E_{ex} is the excitation function at the given excitation wavelength, E_{em} is the normal emission function at the corresponding emission wavelength, c is the analytical concentration, d is the thickness of the sample cell, and K is the characteristic constant comprising the “instrumental geometry factor” and related parameters. Figure 3a–e shows the SFI spectra of HSA–AML in aqueous solution in the pH range 5.4–9.4. The addition of the drug led to a dramatic decrease in the fluorescence intensity of HSA with a weak blueshift (about 1 nm) in the maximum emission wavelength at the investigated concentrations when $\Delta\lambda = 60$ nm at all different pH values. The observed blueshift expresses that the polarity around the Trp residue was decreased and the hydrophobicity was increased; these blueshifts indicate that the conformation of HSA was altered [42]. When pH changed to 5.4, the intensity of the synchronous peak of HSA was 2107, whereas the intensities at other pHs were in the range between 7193 and 8541. This indicated that pH = 5.4 caused a quenching of Trp in HSA to a larger extent than the other pH values. In addition, the relative fluorescence intensity (F/F_0) against drug concentration plots for HSA–AML complex in $\Delta\lambda = 15$ and 60 nm and in the pH range of 5.4–9.4 are displayed in the inset of Fig. 3a–e. Figure 3a–e shows that the slope of quenching plots was higher for $\Delta\lambda = 60$ nm, indicating a significant contribution of the Trp residues in the fluorescence of HSA [37, 43] implying AML was closer to Trp residue compared to Tyr residue at all investigated pH range. The relative intensity of synchronous fluorescence at the range of pH = 5.4–9.4 for $\Delta\lambda = 60$ and $\Delta\lambda = 15$ is shown in Fig. 4a, b, respectively. The most interaction between AML and Trp214 is at pH = 5.4 in section A ($\Delta\lambda = 60$) because the maximum slope is for this pH. Moreover, the slope of curves in section B indicates that Tyr is the less accessible to AML in two pH = 5.4, 7.4, whereas when pH = 9.4, it is further to AML.

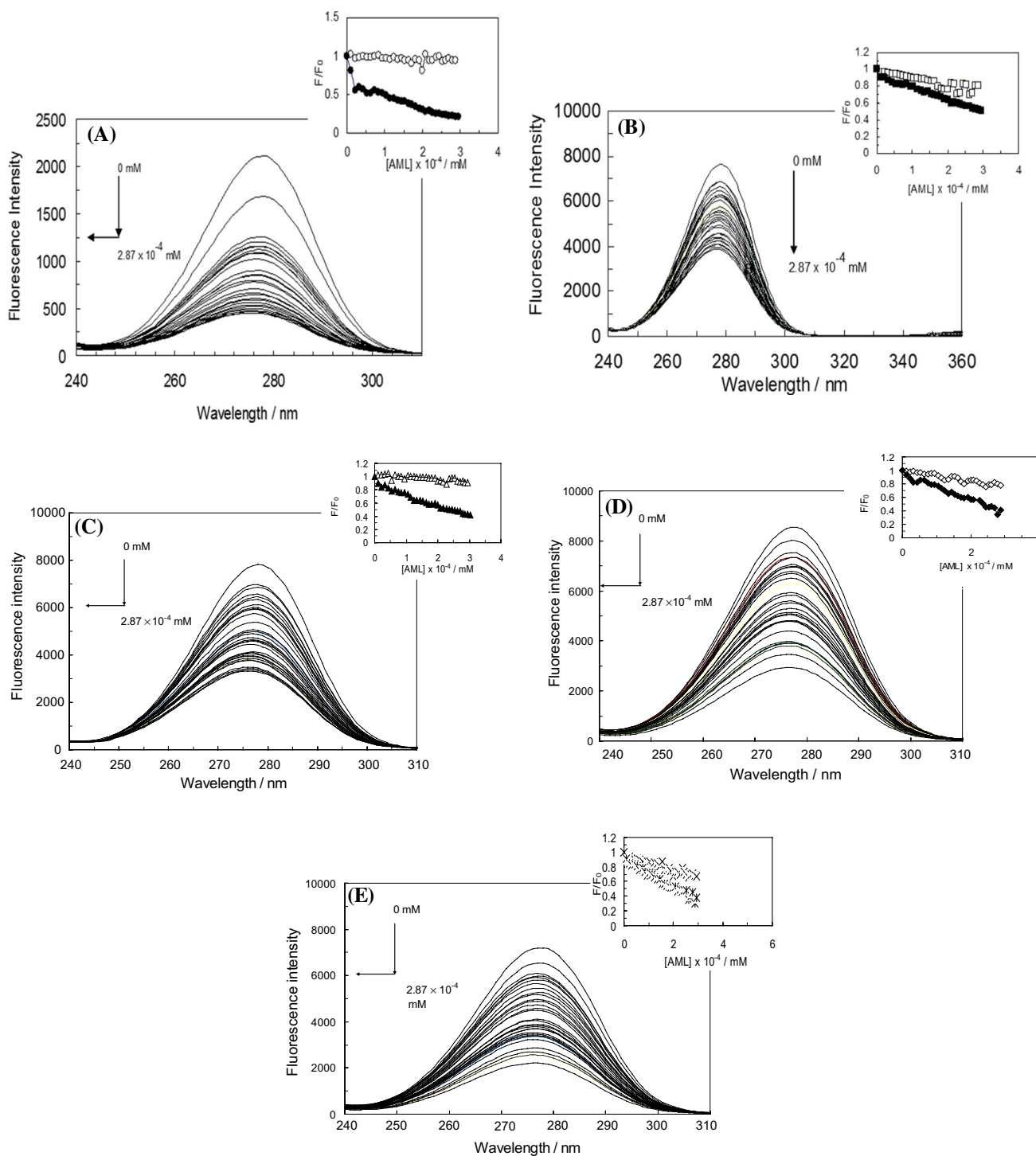


Fig. 3 Synchronous fluorescence spectra of HSA with various contents of AML at $\Delta\lambda = 60$: at pH **a** 5.4, **b** 6.4, **c** 7.4, **d** 8.4, **e** 9.4. The inset for the images, the slopes of F/F_0 versus the concentration of AML for $\Delta\lambda = 15$ nm in sections (A-E) at pH = 5.4 (open circle), 6.4 (open square), 7.4 (open triangle), 8.4 (open diamond), 9.4 (*),

and for $\Delta\lambda = 60$ nm at pH = 5.4 (filled circle), 6.4 (filled square), 7.4 (filled triangle), 8.4 (filled diamond), 9.4 ∇). The concentration of HSA and AML were to 4.59×10^{-6} mM and 2.87×10^{-4} mM, respectively, $T = 298$ K

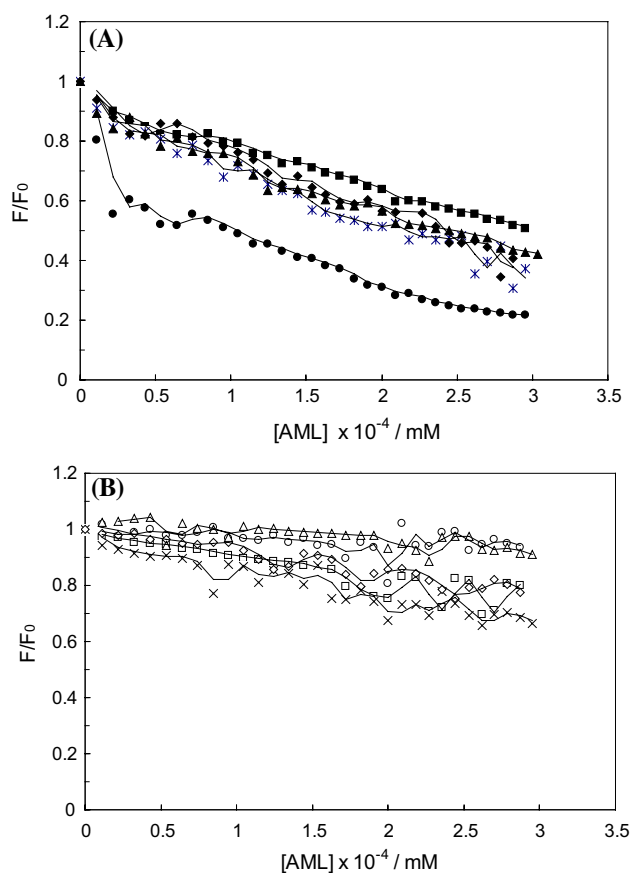


Fig. 4 Effect of increasing AML concentrations on the F/F_0 in the synchronous spectra of HSA in section (A) for $\Delta\lambda = 15$ at pH: 5.4 (open circle), 6.4 (open square), 7.4 (open triangle), 8.4 (open diamond), 9.4 (*) and in section (B) $\Delta\lambda = 60$ at pH: 5.4 (filled circle), 6.4 (filled square), 7.4 (filled triangle), 8.4 (filled diamond), 9.4 †). The conditions of the experiment involved $[HSA] = 4.59 \times 10^{-6}$ mM and $[AML] = 2.87 \times 10^{-4}$ mM, $T = 298$ K

Resonance light scattering spectra (RLS)

According to the theory of Miller, Anglister, and Steinberg, RLS is a scattering–absorption–rescattering process produced by the resonance of scattering and absorption when the wavelength of Rayleigh scattering is located at or is close to its molecular absorption band [43]. The RLS intensity of the HSA–AML system was affected at different pH values and was studied. The results at pH = 7.4 are shown in Fig. 5a. According to Fig. 5a, the RLS intensity of HSA increased when increasing the concentration of AML. The ability of a particle to absorb and scatter light depends on its size, shape, index of refraction relative to the surrounding medium, and scattering. Scattering in each sphere is proportional to the square of the volume, according to the following formula [44]:

$$IRLS = 32\pi^3 V^2 n^2 N \times [(\delta n)^2 + (\delta k)^2] / 3\lambda^4, \quad (14)$$

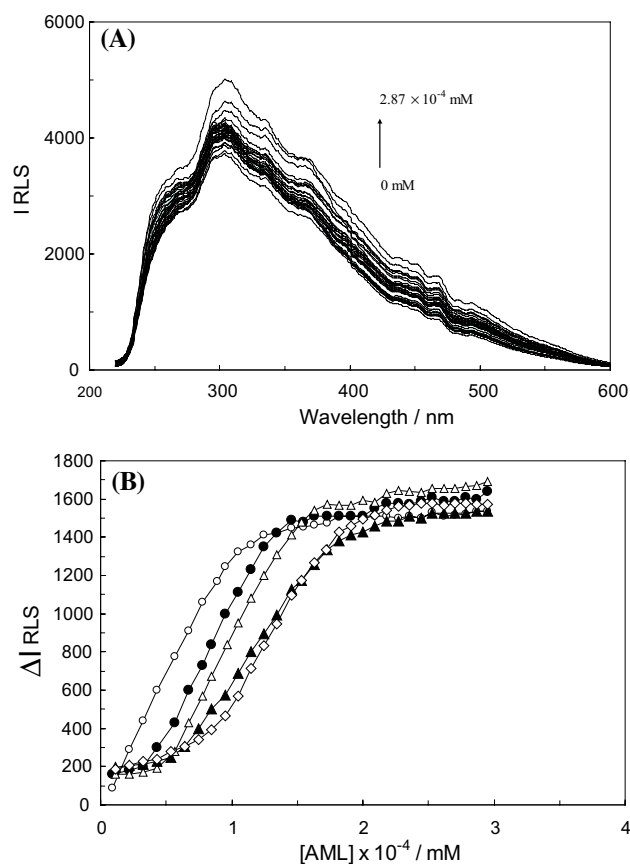


Fig. 5 a, Resonance light scattering spectra of AML–HSA versus the AML concentration at pH = 7.4; (B), ΔI_{RLS} versus the concentration of AML at pH 5.4 (open diamond), 6.4 (filled triangle), 7.4 (open triangle), 8.4 (filled circle), 9.4 (open circle) from 0 to 2.87×10^{-4} mM; $T = 298$ K

here n is the refractive index of the medium, N is the molarity of the solution, λ_0 is the wavelength of the incident and scattered light, V is the square of molecular volume, and δn and δk are the fluctuations in the real and imaginary components of the refractive index of the particle, respectively. With the other factors maintained constant, IRLS is related to the size of the formed particle. The curve in Fig. 5a indicates that the interaction between AML and HSA had occurred and HSA–AML complex was formed and that the derived particles (HSA–AML complex) were greater than HSA and AML alone. Figure 5b shows the curves of ΔI_{RLS} versus the drug concentration in the various pH values, represented as $\Delta I_{RLS} = I_{RLS} - I_{RLS}^0$ (where I_{RLS} and I_{RLS}^0 are the RLS intensities of the systems with and without drug, respectively). Figure 5b displays that with an increasing pH, the C_{CIAC} (critical induced aggregation concentration) decreased, due to AML being a weak alkali and capable of saturating HSA even at low concentrations. On the other hand, this means that the C_{CIAC} point was dependent on the polarity and charges of the solution. Furthermore, at each

pH with an increasing AML concentration, ΔI_{RLS} became enhanced, pointing at the formation of a complex between HSA and AML.

Physicochemical characterization of the complex

A biomaterial's zeta-potential indicates its electric surface properties. The zeta-potential is measured by electrophoresis or alternatively by streaming potential methods [45]. Figure 6a shows a plot of the zeta-potential as a function of the drug concentration at pH values between 5.4 and 9.4. As follows from the figure, at all pH values the protein consisted of negative charges, and with addition of AML, the zeta-potential increased, which is indicative of the existence of electrostatic interactions between HSA and the AML molecules [46]. Also in maximum point of curves, the value of zeta-potential was decreased in response to adding more AML concentration which indicates that the AML molecules could bind to HSA via hydrophobic forces [17]. Moreover,

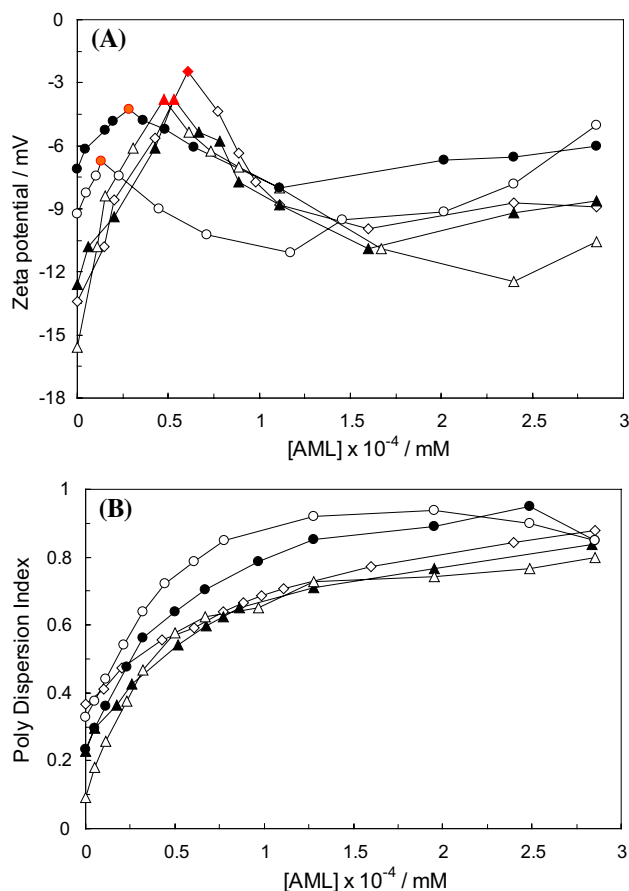


Fig. 6 a Effect of AML on the (a), ζ -potential, b the polydispersity index of HSA at pH 5.4 (open diamond), 6.4 (filled triangle), 7.4 (open triangle), 8.4 (filled circle), 9.4 (open circle), [HSA] = 4.59×10^{-6} in phosphate potassium buffer; [AML] = 2.87×10^{-4} mM; T = 298 K

probably the observed decrease in zeta-potential values is through turned up two acidic amino acids (Asp, Glu) in the surface of protein. These maximum points correspond to an initial point of aggregation, implying that the HSA surface was full and that AML aggregation occurred [17]. Figure 6a illustrates that HSA in pH = 5.4 and 9.4 saturates with the most and least concentration of AML, respectively, from which these observations confirm the obtained result of CCIAC in ΔI_{RLS} curves.

The size analysis indicated that cationic modification had minor effects on the size distributions of the protein [47]. Many proteins are monodisperse, signifying that they have a single molecule size. However, a synthetic polymer, which consists of a mixture of molecules, is most often polydisperse. The relation between weight average molar mass and the number average molar mass, M_w/M_n , is called the heterogeneity index (or “polydispersity index”). It is achieved from the following [48]:

$$M_w = 1/m \sum m_i M_i \quad (15)$$

$$M_n = 1/N \sum N_i M_i, \quad (16)$$

where m is the total mass of the sample, m_i is the total mass of molecules of molar mass M_i , N_i is the number of molecules with molar mass M_i , and N is the total number of molecules.

The relation between PDI and concentration of AML for all pHs is shown in Fig. 6b. As can be seen, the PDI increased with increasing AML concentration in the HSA–AML complex, indicating that the size of the complexes became bigger, which constituted of various molecules or increase in heterogeneity in system. This means that the heterogeneity of the HSA–AML complex in solution depended on the pH behavior. Figure 6b shows that for an increasing amount of negative charges at high pH, the PDI values increased. This corresponded to the negative charges affecting the HSA structure which caused different interactions with AML. Moreover, the maximum amount of PDI was found at pH 5.4 and 9.4 due to an enhancement of the acidity or alkali potency increasing the charge of molecules and resulting in a higher zeta-potential and PDI. Above these concentrations in five pH values, new compound is not added in the system because PDI stabilized with increasing of AML.

Three-dimensional fluorescence spectroscopy

Three-dimensional fluorescence spectroscopy is a new analytical technique applied to investigate the conformational changes of proteins [49]. The maximum emission wavelength and the fluorescent intensity of the residues have a close relation to the polarity of their microenvironment [50]. The excitation wavelength, the emission wavelength, and

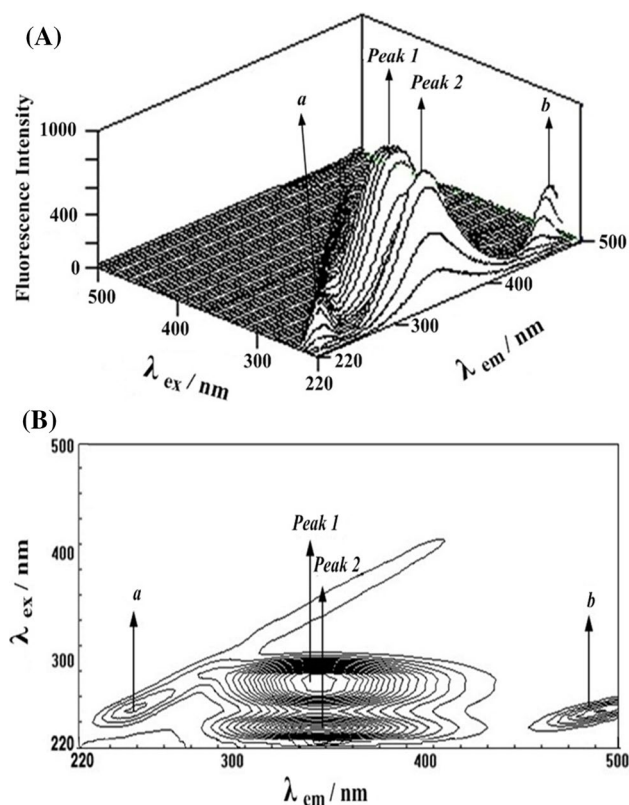


Fig. 7 **a** Three-dimensional spectra of HSA; **b** contour spectra of HSA at pH = 7.4 with the ratio of HSA–AML equal to 1:1; [HSA] = 4.59×10^{-6} mM, [AML] = 0 to 2.87×10^{-4} mM and T = 298 K

the fluorescence intensity can be used as the axes in order to investigate the synthetic information of the samples. If there is a shift at the excitation wavelength or at the emission wavelength around the fluorescent peak, appearance of a new peak, disappearance of existing peak(s), and so on, it could be an important evidence to suggest conformational changes upon the HSA. Figure 7a presents three-dimensional fluorescence spectra at pH = 7.4 at a ratio 1:20 of HSA–AML. Here, peaks a and b are the Rayleigh scattering peak ($\lambda_{ex} = \lambda_{em}$) and the second-order scattering peak ($\lambda_{em} = 2\lambda_{ex}$), respectively, appearing with the “chine” pattern. The fluorescence intensity of peak a increased with the addition of AML as the complex between AML and HSA was formed and the diameter of the macromolecule increased in turn causing an enhanced scattering effect [7]. Also, two typical fluorescence peaks with aspects of “humps” could be easily observed. These were peak 1 (fluorescence peak) and peak 2 (second-order fluorescence peak). The corresponding characteristic parameters for other pH values at a ratio of 1:1 of HSA–AML are listed in Table 3.

Peak 1 ($\lambda_{ex} = 285$ nm/ $\lambda_{em} = 344$ nm) mainly revealed the spectral characteristic of the Trp and Tyr residues, since when the protein is excited at 280 nm, it mainly displays the intrinsic fluorescence of the Trp and Tyr residues, and the fluorescence of Phe residue is negligible [51, 52]. Peak 2 ($\lambda_{ex} = 235$ nm/ $\lambda_{em} = 344$ nm) exhibits the fluorescence of the polypeptide backbone structure, which is mainly caused by the transition of $\pi \rightarrow \pi^*$ of HSA’s characteristic polypeptide backbone structure C = O [53]. Table 3

Table 3 Three-dimensional fluorescence characteristics of HSA–AML at a molar ratio of 1:20

System	Peak	Peak position, $\lambda_{ex}/\lambda_{em}$ (nm/nm)	Stokes $\Delta\lambda$ (nm)	Intensity
pH = 5.4	Rayleigh scattering peak	255/255	0	174.494
	Fluorescence peak	285/339	56	629.626
	Second-order scattering	245/490	λ_{ex}	236.348
	Second-order fluorescence peak	235/338	103	582.579
pH = 6.4	Rayleigh scattering peak	250/250	0	180.463
	Fluorescence peak	285/345	60	949.036
	Second-order scattering	250/500	λ_{ex}	229.123
	Second-order fluorescence peak	235/344	109	741.894
pH = 7.4	Rayleigh scattering peak	250/250	0	193.399
	Fluorescence peak	285/344	59	867.873
	Second-order scattering	250/500	λ_{ex}	227.579
	Second-order fluorescence peak	235/344	109	834.866
pH = 8.4	Rayleigh scattering peak	255/255	0	155.775
	Fluorescence peak	285/332	47	432.834
	Second-order scattering	250/500	λ_{ex}	210.845
	Second-order fluorescence peak	235/330	95	453.102
pH = 9.4	Rayleigh scattering peak	255/255	0	150.43
	Fluorescence peak	285/340	57	498.387
	Second-order scattering	250/500	λ_{ex}	212.541
	Second-order fluorescence peak	235/339	106	412.344

illustrates the three-dimensional fluorescence characteristics of HSA–AML complex at a molar ratio of 1:20 in the pH range of 5.4–9.4. Since pH = 7.4 is similar to physiological conditions, we compare the obtained results in other pH with pH = 7.4. As can be seen from Table 3, the strength of peak a (RLS) at pH = 7.4 is significantly greater than basic and acidic pH, and thus the larger HSA–AML complex was formed at pH = 7.4. In addition the fluorescence intensity of peak 2 decreased obviously after changing pH value from 7.4 to basic and acidic pH. These observations clarified that changing the pH value induced the unfolding of the peptide chain, and then structure of HSA was altered and has been affected by altering pH. Analyzing from the fluorescence intensity of peak 1 displays an obvious blueshift in λ_{em} max, which suggests that the polarity around the Trp and Tyr residue was decreased and hydrophobicity was increased during altering pH.

Quenching at pH = 7.4 was more significant than at the other pH. In section B of Fig. 7, a contour map of HSA–AML is shown. AML thus quenched the fluorescence of HSA to different degrees, which indicated that a complex was possibly formed between AML and HSA changing the conformation of the latter.

Measurement of red edge excitation shift (REES)

Recently, we demonstrated that the magnitude of REES of a fluorophore can be used as a parameter when studying the photophysical and chemical properties of the formation of complexes [53]. However, REES is observed with polar fluorophores in motionally restricted media, such as very viscous solutions or condensed phases [54]. REES represents a powerful approach that can be used to directly monitor the environment and dynamics around a fluorophore in a complex biological system [55]. REES represents a shift in the wavelength of the maximum fluorescence emission toward higher wavelengths, caused by a shift in the excitation wavelength toward the red edge (longer wavelengths) of the absorption band. In fact, the origin of REES lies in the change in fluorophore–solvent interactions in the ground and excited states and occurs when there is a slow relaxation of the solvent medium [56].

In the present study, we investigated the REES effect in the HSA–AML system at different pH when exciting Trp at both 280 and 295 nm, and the results are listed in Table 4. The value of $\Delta\lambda_{em, max}$ is defined as the difference of the emission maximum for an excitation at 295 nm as opposed to 280 nm. At pH = 7.4, the maximum of $\Delta\lambda_{em, max}$ equaled 3 and 4 at ratios of 1:1 and 1:5, respectively, for the HSA–AML system. This indicates an obvious impact of AML on the mobility of the Trp. Also the Trp residue faced more restrictions from its surroundings in the HSA–AML system at this pH. A comparison between two acidic and

Table 4 Summary of the red edge excitation for HSA–AML at molar ratios of 1:1 and 1:5 in the pH range of 5.4–9.4; T:298 K

system	$\Delta\lambda_e$ /nm	$\Delta\lambda_b$ /nm
pH = 5.4	– 1	– 1
pH = 6.4	1	0
pH = 7.4	3	4
pH = 8.4	2	3
pH = 9.4	2	3

^aREES is the difference between emission maxima obtained at 295 and 280 nm excitation at the ratio 1:1 for HSA–AML

^bREES is the difference between emission maxima obtained at 295 and 280 nm excitation at the ratio 1:5 for HSA–AML

basic media indicated that in the basic media, the Trp residue faced more restrictions from its surroundings and that the mobility of the Trp residue in acidic media thereby was more significant than in the basic ones. Thus, a considerable change in conformation took place at acidic pH. On the other hand, the $\Delta\lambda_{em, max}$ values were negative and zero at pH = 5.4 and a ratio of 2, as well as at pH = 6.4 for a ratio of 1:5. This indicated that at low pH, the single Trp was located in a somewhat rigid, solvent-restricted environment at these pH values, demonstrating a lower mobility than at the other pH [53]. The other noticeable point observed was that with an increase in AML, the REES increased, suggesting that the binding of AML to HSA occurred through an increasing hydrophobicity around the Trp residue or a more significant restriction of the Trp moieties.

Static quenching due to an excited-state complex formation/FRET

The first quantitative test of the Förster theory and the crucial experiment that put FRET on the map of biochemistry were published by Stryer and Haugland in 1967 [57]. FRET is widely used to determine proximities, distances, orientations, and dynamic properties of biomolecular structures, and its theory has been described in numerous reviews [58]. AML can quench the intrinsic fluorescence of HSA remarkably through binding, which suggests the occurrence of energy transfer between the fluorophores in HSA and AML. FRET is very useful for realizing spatial distributions with regard to structure and conformation of donor–acceptor complexes [34]. The efficiency of FRET depends mainly on the following factors [37, 54]: 1. The extent of overlap between the donor emission and the acceptor absorption spectra. 2. The relative orientation of the donor and acceptor dipoles. 3. The distance between the donor and the acceptor; here, the donor and acceptor are HSA and AML, respectively. 4. Using FRET, the efficiency of energy transfer (E) can be expressed by the following equation [36]:

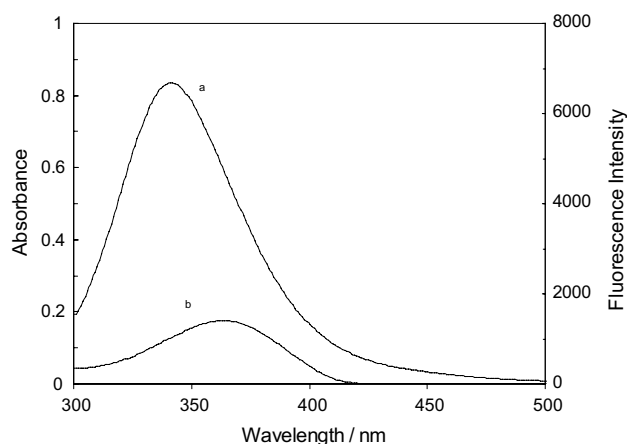


Fig. 8 Overlap of the UV absorption spectrum of HSA **a** with the fluorescence emission spectrum of AML **b** at pH: 7.4; [HSA] = 4.59×10^{-6} mM; [AML] = 2.87×10^{-4} mM and T = 298 K

Table 5 Distance between HSA (donor) and AML (acceptor) according to FRET at pH = 5.4–9.4; T = 298 K

System	<i>r</i> /nm
HSA–AML (pH 5.4)	2.27
HSA–AML (pH 6.4)	2.11
HSA–AML (pH 7.4)	1.92
HSA–AML (pH 8.4)	1.83
HSA–AML (pH 9.4)	2.08

$$E = R60/(R60 + r6), \quad (17)$$

where *r* is the average distances between a donor and an acceptor, and R0 is the critical distance at which the transfer efficiency is 50% and can be calculated from [52]:

$$R60 = 8.8 \times 10^{-25} K2\phi n - 4J, \quad (18)$$

where K2 is the space factor of orientation, *n* is the refractive index of the medium, ϕ is the fluorescence quantum yield of the donor, and *J* is the effect of the spectral overlap between the emission spectrum of the donor and the absorption spectrum of the acceptor, which can be calculated according to:

$$J = \int F(\lambda)\epsilon(\lambda)\lambda^4 d\lambda / \int F(\lambda)d\lambda. \quad (19)$$

Here, F(λ) is the fluorescence intensity of the donor at wavelength λ , and $\epsilon(\lambda)$ is the molar absorption coefficient of the acceptor at λ .

Figure 8 shows a spectral overlap between the fluorescence emission spectrum of HSA and UV–Vis absorption spectrum of AM at pH = 7.4, and the distances between donor (HSA) and acceptor (AML) in the pH range between 5.4 and 9.4 are listed in Table 5. As can be observed, the distance between them was less than 8 nm, which indicated that the energy transfer from HSA to AML occurred with a high probability. Moreover, the less distance between Trp214 and

AML binding site was observed at pH = 8.4 and 7.4, and thus more stable HSA–AML complex is formed at these pH values. Also, these results indicated a static quenching interaction between AML and HSA and the formation of an excited-state complex which could result in the transfer of some of the excited energy of the fluorophore (the donor) to an acceptor.

Changes of the protein's secondary structure induced by drug binding

In order to better understand the conformational changes of HSA upon the addition of AML, circular dichroism (CD) was performed on HSA and the HSA–AML system. CD measurements can be divided into the following classes: 1. Far UV-CD (below 260 nm): arising from peptide bonds and 2. Near UV-CD (260–310 nm): where aromatic side chains and cystine (disulfide bridges) exhibit absorption [59].

The far UV-CD spectrum originates primarily from the asymmetric juxtaposition of the backbone amide groups of the peptide chain in the folded state [60]. However, backbone amide groups may not be the sole contributor to the observed far UV-CD signal of a folded polypeptide chain. Contributions from side-chain chromophores, especially Phe, Tyr, AND Trp, can potentially alter the overall far UV-CD signal if they are locked in asymmetric geometries, due to favorable interactions with the backbone [61]. The types of information which can be obtained from CD studies of proteins include [32, 62]:

1. Secondary structure composition (% α -helix, β -sheet, turns, etc.) from the peptide bond region.
2. Tertiary structure fingerprint.
3. Integrity of cofactor binding sites.
4. Conclusion about the overall structural features of the protein.
5. Conformational changes in the protein.
6. Protein folding.
7. CD as a structural technique compared with X-ray and NMR approaches.

First, we recorded the far UV-CD spectra of HSA–AML from 200 to 240 nm in a phosphate buffer at varying pH. The far UV-CD spectrum displayed minima at 208 and 222 nm, consistent with an abundance of α -helical structure, rationalized by the $n \rightarrow \pi^*$ transition in the peptide bond of the α -helix [63] (data not shown). The addition of AML at varying concentrations substantially reduced the amount of α -helical structure as seen by the lower minima at 208 and 222 nm, arising from an unfolding process that the protein underwent in the presence of excess drug molecules and suggesting the change of the HSA secondary structure. This might be induced by the formation of the HSA–AML

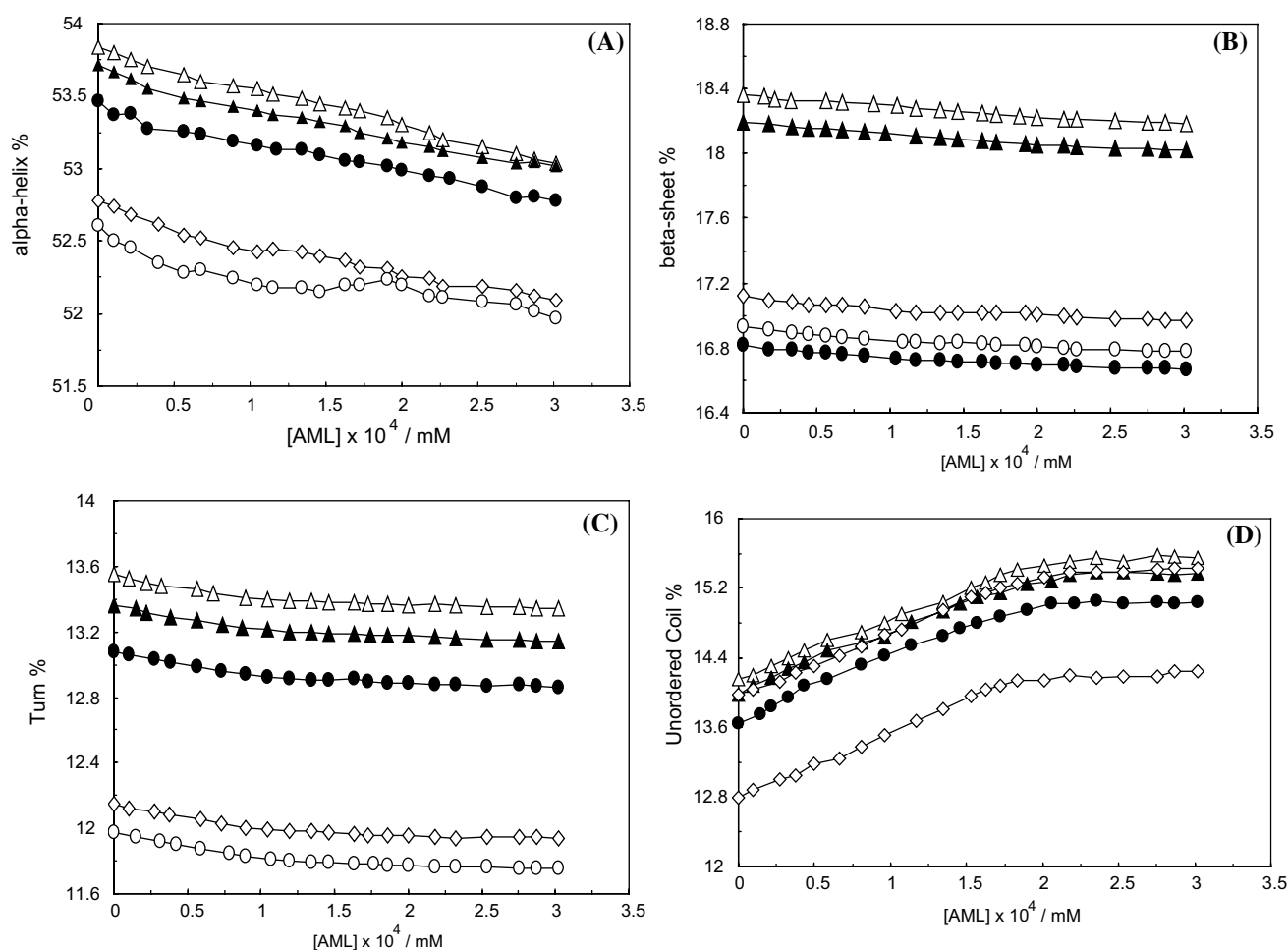


Fig. 9 Fraction of differences with regard to the secondary structures in **a** α -helix; **b** β sheet; **c** turn and **d** unordered coil of HSA with a concentration of AML from 0 to 2.87×10^{-4} mM in a fixed concen-

tration of HSA = 4.59×10^{-6} mM at pH = 5.4 (open diamond), 6.4 (filled triangle), 7.4 (open triangle), 8.4 (filled circle), 9.4 (open circle) and T = 298 K

complex. Figure 9a–d demonstrates the dependence of the secondary structure, which involved α -helix, β -sheet, turn and unordered coil fractions of HSA, as a function of the concentration of AML at various pH values. Figure 9 shows that most of the fraction of α -helix, β -sheet, and turn decreased in the presence of AML and that the fraction of unordered coil increased with increasing AML concentrations. These results imply that the effect of AML upon HSA changed secondary structure of the protein and with the loss of helical stability [19]. At pH = 7.4 and basic pH, results pointed to, respectively, the highest and lowest fractions of secondary structures as compared to at the other pHs.

Computational modeling of HSA–AML

Binding domain

Although solution experiments may more closely represent physiological conditions when attempting to obtain

information of the right site and interaction forces of AML binding to HSA, AutoDock 4 was applied to deduce the binding mode between the two substances [38]. According to the description of the 3D structure of crystalline albumin, HSA comprises three homologous domains (I–III): I (residues 1–195), II (196–383), and III (383–585). Furthermore, each domain has two sub-domains (A and B), which consisted of six (sub-domain A) and four (sub-domain B) α -helices.

Despite a very high stability, HSA is a flexible protein with the 3D structure susceptible to environmental factors such as pH, ionic strength. Recent studies have shown that HSA is able to bind multiple ligands in several binding sites [64]. There is a large hydrophobic cavity present in sub-domain IIA that many drugs can bind to. Almost all hydrophobic amino acids are embedded in the cylinders forming hydrophobic cavities, and only the tryptophan residue Trp214 of HSA is in sub-domain IIA, which plays an

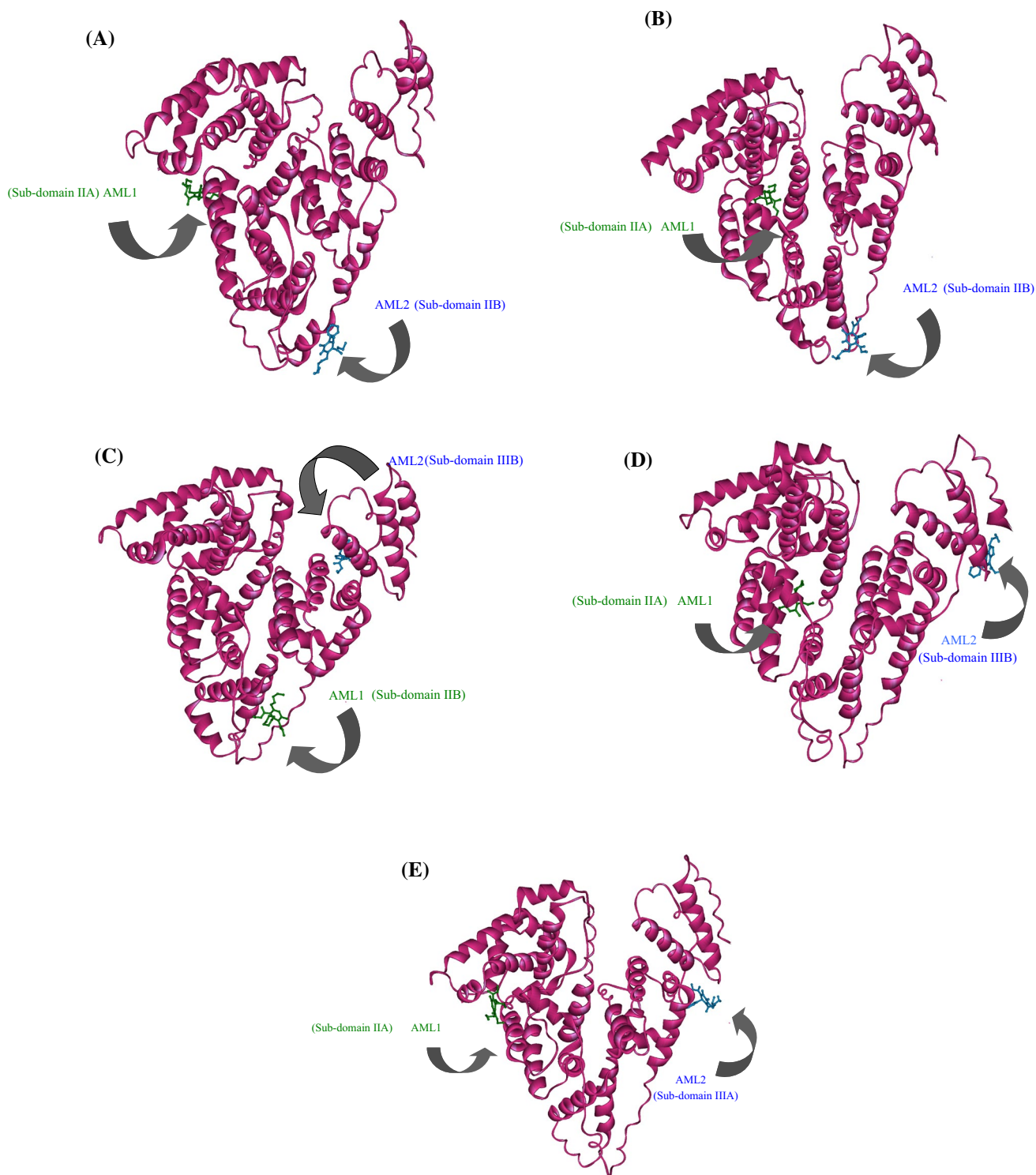


Fig. 10 Computational model of AML docked in HSA. **a–e** shows docking at pH = 5.4, 6.4, 7.4, 8.4 and 9.4. HSA is represented as a solid ribbon colored in violet. The structure of the ligands is shown

in a ball and stick representation, dark green and dark blue for AML1 and AML2, respectively

important role in absorption, metabolism, and transportation of biomolecules [1, 38, 37].

The best ranked results from the docking study are shown in Fig. 10a–e in the pH range 5.4–9.4. The important point from this figure is that, in most cases, AML binds to

sub-domain IIA (site I) and IIIB, which is emphasized in this study. The obtained results for binding energy and inhibition constant are summarized in Table 7 and demonstrate that the minimum inhibition constant and more binding energy (best result of docking) was observed at pH = 8.4 ($K_{i1} = 26.62$ and $K_{i2} = 20.3$ mM, $Be_1 = -6.26$ and $Be_2 = -2.31$) and then at pH = 7.4 ($K_{i1} = 40.67$ and $K_{i2} = 48.71$ Mm). It can be seen that AML was first situated within sub-domain IIA in Sudlow's site I and then bound to sub-domain IIIB when pH = 8.4. Because a pH of 7.4 is similar to physiological conditions, it was a candidate for further. AML was located in sub-domain IIB and IIIB of HSA in two steps of binding and was adjacent to hydrophobic and hydrophilic residues that—in the 12-Å environment of AML (Fig. 11a, b)—caused binding of AML with hydrophobic amino acids via hydrophobic and van der Waals forces. In the first binding site of AML, the protein had five residues with positive charge (Lys225, Arg336, Arg337, His338, and Lys378), four residues with negative charge (Asp296, Asp301, Glu333, and Asp340), and the rest were polar residues (e.g., Gln221, Asn295, Gln385) playing an important role in stabilizing the

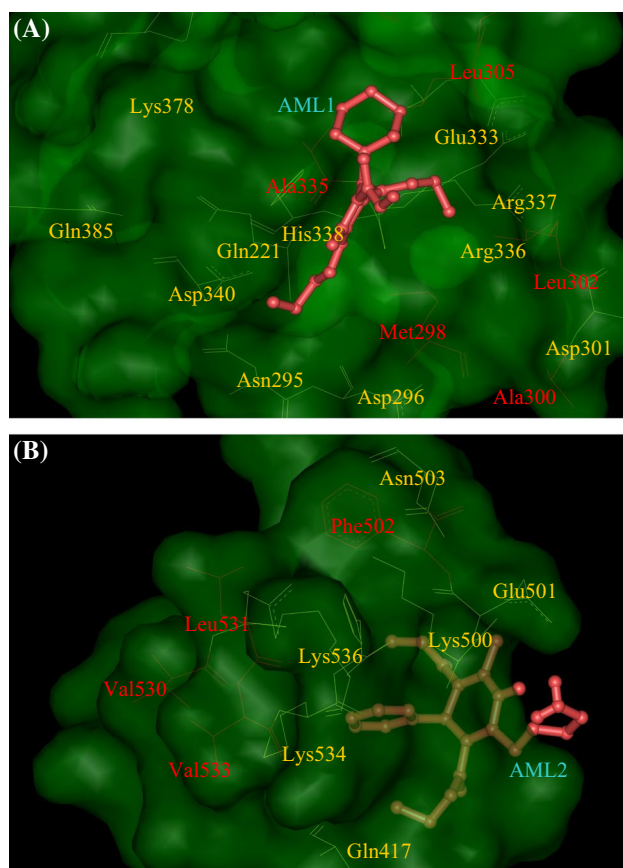


Fig. 11 Co-crystal structure of HSA and AML. AML1 and AML2 exist in the binding site IIB and site IIIA of HSA with hydrophobic and hydrophilic amino acids around 12Å. AML is shown in a ball and stick representation

complex of ligands such as AML via H-bonds and electrostatic interactions with HSA.

Similar observations were found for the second docked AML in Fig. 11b. It is important to note that Trp214 exists at a certain distance (1.87 and 3.09 nm) from the first and second molecules of AML in sub-domains IIB and IIIB. Here, the distance to the first AML was similar to that observed from FRET donor and acceptor analysis (1.92 nm), thus supporting the idea of the formation of an HSA–AML complex (Fig. 12a). The calculated distances between Trp214 and

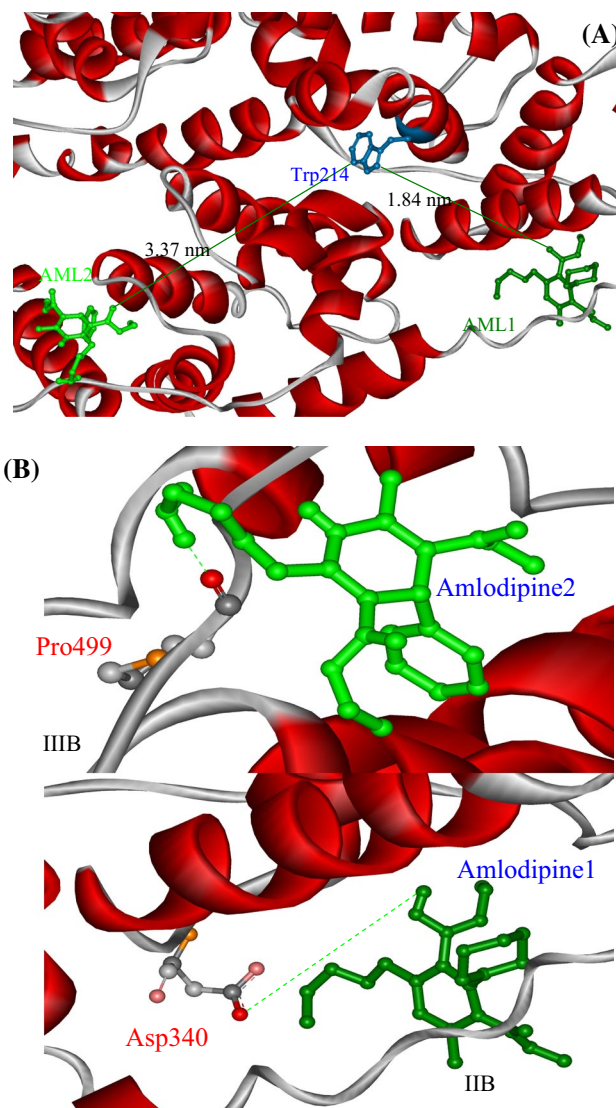


Fig. 12 a Distance between Trp214 of HSA and two AML at pH = 7.4; Trp214 is shown in a ball and stick representation in dark blue; the distance between Trp214 and AML is represented in dye; b The hydrogen bond is indicated by dashed lines, the structure of HSA is represented as a solid ribbon; Asp340 and Pro499 are shown in ball and stick representations as are the two drugs—dark and light green for AML1 and AML2, respectively, while the two H-bonds are introduced as dashed lines

Table 6 Distance between HSA (donor) and AML (acceptor) according to molecular modeling at pH = 5.4–9.4

pH	System	r/nm
5.4	HSA–AML1	2.33
	HSA–AML2	3.61
6.4	HSA–AML1	2
	HSA–AML2	2.09
7.4	HSA–AML1	1.80
	HSA–AML2	3.05
8.4	HSA–AML1	1.69
	HSA–AML2	4.05
9.4	HSA–AML1	2.23
	HSA–AML2	2.62

AML binding sites for other pH values are shown in Table 6 and were in good correlation with the experimental results.

Figure 12b also displays hydrogen binding for the HSA–AML complex, which is obviously important for the system's stability. A comparative table of experimental and theoretical results (Table 7) shows a good correlation between K_{sv} (Stern–Volmer constant) and K_i (Inhibition constant) in both AML binding sites which K_{sv} had an opposite relation with K_i . For example, with increasing the value of pH from 8.4 to 9.4, the value of K_{sv} was decreased (pH = 8.4 presented the uttermost quantity of K_{sv} that $K_{sv1} = 21.33 \times 10^4 \text{ M}^{-1}$ and $K_{sv2} = 21.86 \times 10^4 \text{ M}^{-1}$, whereas at pH = 9.4 $K_{sv1} = 8.81 \times 10^4 \text{ M}^{-1}$ and $K_{sv2} = 8.61 \times 10^4 \text{ M}^{-1}$), and hence the binding affinity between AML with HSA remarkably is reduced, but the reversal fact was observed for the value of K_i that determined from the docking studies. The value of K_i significantly increased when pH was reached to 9.4 (at pH = 8.4 $K_{i1} = 26.62 \text{ } \mu\text{M}$, $K_{i2} = 20.3 \text{ mM}$ whereas at pH = 9.4 $K_{i1} = 54.8 \text{ } \mu\text{M}$ and $K_{i2} = 112.56 \text{ mM}$).

It can be seen from the results that the best binding occurred at pH = 8.4 and the worst was at pH = 9.4. The discrepancy between the theory and experimental results is due to the fact that $K_{sv2} > K_{sv1}$; however, $K_{i2} < K_{i1}$, which is a consequence of the second minimization of binary complex with the HyperChem software. Proteins prefer to condense as much as possible when minimized by software. This fact makes them different from their natural

Table 8 Values of RMS between proteins at different pH = 5.4–9.4 with 1AO6

pH	RMS	Number of atoms involved
5.4	1.28 Å	2264
6.4	1.13 Å	2288
7.4	1.15 Å	2300
8.4	1.08 Å	2288
9.4	1.17 Å	2300

counterparts and further docking results may be different from what is expected. The docking results confirmed the distances of AML with Trp214 of HSA that were observed from the experimental analysis. Moreover, a comparison of natural and minimized proteins at different pH showed little differences from an RMS point of view and demonstrate in Table 8. Three reasons are assumed to explain these results. A. pH has little effect on HSA folding. B. The method used for this calculation needs to be adapted to ternary systems. C. Despite these discrepancies in the results, it was still possible to rely on them due to the small difference of the proteins' pHs which were lower than the resolution of the original protein retrieved from the PDB site. At pH = 5.4 and pH = 8.4, the protein revealed the largest and lowest RMS, respectively, which reflects its significance as opposed to feeble structural change.

Multiple alignments

Multiple alignments are a way to detect the most conserved residues within a protein or gene. This identity then reflects the importance of the related parts that are usually known as active or binding sites. The technique was utilized in our study to investigate probable binding sites of HSA, and the results are presented in Scheme 2. There was a good correlation between the multiple alignments and docking method, in which the conserved areas of multiple alignments were in the vicinity of those extracted from the docking study. For example, Asp340 that was hydrogen-bonded with AML

Table 7 Values of K_{sv1} and K_{sv2} from experimental analysis and K_{i1} , K_{i2} , and the binding energy achieved from interaction of AML with HSA by molecular modeling at pH = 5.4–9.4

pH	$K_{sv1}^a \times 10^{-4}/\text{M}^{-1}$	$K_{sv2}^a \times 10^{-4}/\text{M}^{-1}$	Be_1^b	Be_2^b	K_{i1}^c/mM	K_{i2}^c/mM
5.4	10.290	14.16	– 5.85	– 1.47	51.68	83.65
6.4	11.454	12.47	– 5.90	– 1.46	47.08	84.61
7.4	19.742	20.33	– 5.99	– 1.79	40.67	48.71
8.4	21.329	21.86	– 6.26	– 2.31	26.62	20.3
9.4	8.81	8.61	– 5.81	– 1.29	54.8	112.56

^aStern–Volmer constant

^bBinding energy

^cInhibition constant

```

332 DFVESKDVCKNYAEAKDVFLGMFLYEYARRHPDYSVLLRLAKTYETTLEKCCAAADPHECYAKVFD-- 399 P02768 ALBU_HUMAN
332 DFVSGKDVCKNYAEAKDVFLGMFLYEYARRHPDYSVLLRLAKTYETTLEKCCAAADPHECYAKVFD-- 399 Q56G89 Q56G89_HUMAN
341 DFVESKDVCKNYAEAKDVFLGMFLYEYARRHPDYSVLLRLAKTYETTLEKCCAAADPHECYAKVFD-- 408 B4DPP6 B4DPP6_HUMAN
324 DYVESKDVCKNYAEAKDVFLGMFLYEYARRHPDYSVLLRLAKAYEATLEKCCAAADPHECYAKVFD-- 391 Q28522 ALBU_MACMU
332 DFVEDKEVCKNYQEAKDVFLGTFLYEYSRRHPEYSVSLLLRLAKEYEATLEKCCATDDPPACYAHVFD-- 399 P49064 ALBU_FELCA
331 DFVEDKEVCKNYKEAKHVFLGTFLYEYSRRHPDYSVSLLLRIAKIYEATLEDCCKEDPPACYATVFD-- 398 P08835 ALBU_PIG
331 DFAEDKEVCKNYQEAKDVFLGSLYEYSRRHPEYAVSLLRLAKEYEATLEDCCKEDPHACYATVFD-- 398 P14639 ALBU_SHEEP
332 EFVEDKDVCKNYEEAKDLFLGKFLYEYSRRHPDYSVLLRLGKAYEATLKKCCATDDPHACYAKVLD-- 399 P49065 ALBU_RABIT
307 DYVEDKDVCKNYQEAKDIFLGTFLYEYSRRHPEYSAFLLRLIAKEYEATLERCCAAADPHACYAKVLD-- 374 Q6B320 Q6B320_ELEMA
336 KYIEDKEVCKSFEAGHDAPMAEFVYEYSRRHPEFSIQLIMRIAKGYESLLEKCKTDNPAECYANAQE-- 403 P19121 ALBU_CHICK
338 EFIEDKGCERFAQEKDTHLARFLYEYSRRHPEFSAQMLLRIGKGYEDLLECCCKTGSPDNCCSRGEE-- 405 E1BV96 E1BV96_CHICK
328 VHADIAAVCQTFTKTPDVAMGKLVYEISVRHPESQVILRFAKEAEQALLQCCDMEDHAECVKTALAGS 397 Q03156 ALBU_SALSA
.      *: : .  . : ** : ***: : :*:.* * * ** . *

```



Scheme 2 Multiple alignments of the binding of AML to HSA in two steps

according to the docking study was within the conserved area from K23 to E54, which is indicated with two circles. Another example is AML2, with hydrogen bonding to Pro499, which lay in the conserved area from C514 to R35.

Prediction of binding sites

To investigate and support the results from the docking study, we employed a sequence analysis method that could predict binding sites from sequence. For this purpose, we used the 3D ligand site. Analysis of the HSA sequence by this site revealed that Gln33 lay in a conserved area thus supporting the idea of a binding site of HSA at pH 5.4. Other areas that were highlighted by the 3D ligand site were those around amino acids Pro106, Phe145, leu150, and Tyr157, which supports the data from the docking analysis.

We also used the MEdock site which accepts pdb files of proteins and ligands in order to calculate possible sites of binding for the given substances. The site returned five docking results in which the first was always the best in terms of docking energy. The data are reported in Table 9. Also this method confirmed the predicted results by the main docking method (i.e., AutoDock).

Predicted binding site

Residue	Amino acid	Contact	Av distance	JS divergence
33	GLU	2	0.52	0.43
106	PRO	2	0.38	0.36
108	LEU	2	0.27	0.30
111	LEU	2	0.00	0.47
118	VAL	2	0.60	0.38

Residue	Amino acid	Contact	Av distance	JS divergence
119	MET	3	0.00	0.30
120	cys	2	0.00	0.76
121	THR	2	0.00	0.33
122	ALA	2	0.00	0.41
123	PHE	2	0.00	0.53
124	HIS	2	0.00	0.34
125	ASP	2	0.00	0.39
126	ASN	2	0.00	0.49
127	GLU	2	0.05	0.34
128	GLU	2	0.00	0.26
129	THR	2	0.00	0.17
130	PHE	4	0.00	0.53
131	LEU	4	0.00	0.36
132	LYS	3	0.01	0.20
133	LYS	3	0.03	0.34
134	TYR	4	0.00	0.67
135	LEU	2	0.00	0.52
137	GLU	2	0.00	0.06
138	ILE		0.00	0.43
139	ALA	2	0.00	0.64
140	ARG	2	0.26	0.57
141	ARG	2	0.00	0.59
142	HIS	2	0.00	0.66
143	PRO	2	0.00	0.61
145	PHE	2	0.29	0.39
150	LEU	2	0.00	0.52
157	TYR	3	0.00	0.66

Table 9 Results of MEdock with distances of AML1 and AML2 as well as the lowest docked energy

pH	distance	Lowest docked energy	Download link
5.4	20.76	– 7.47	https://medock.csie.ntu.edu.tw/buf/27686/1me1.pdb
6.4	17.06	– 6.62	https://medock.csie.ntu.edu.tw/buf/dafc2/1me1.pdb
8.4	21.61	– 6.40	https://medock.csie.ntu.edu.tw/buf/1d22c/1me1.pdb
9.4	10.81	– 6.76	https://medock.csie.ntu.edu.tw/buf/b25f3/1me1.pdb

Conclusions

The interaction between AML and HSA has been investigated in vitro under varying pH conditions. An approach for studying the binding of AML to HSA was provided based on different optical techniques and molecular modeling. The fluorescence titration results showed that the binding occurred via two types of binding sites. The change in protein conformation upon binding, especially in the environment of the aromatic residues, was monitored as a function of added drug by synchronous, CD and three-dimensional fluorescence spectroscopies. The results indicated that the structure of the environments of the Trp and Tyr residues was altered and that the physiological functions of HSA were affected by AML. Due to the interaction between AML and HSA, large complexes were formed and gave rise to an increase in RLS. All these experimental results and theoretical data revealed that AML could bind to HSA and be effectively transported and eliminated in the body. This represents a useful guideline for further toxicological investigations. Additionally, docking calculations determined that AML was located in the vicinity sub-domains IIA and IIIB upon HSA molecule. The present study is of great importance for the fields of pharmacy, pharmacology, and biochemistry since it provides important information for clinical research as well as a theoretical basis for designing new drugs.

Acknowledgements The financial support of the Research Council of the Mashhad Branch, Islamic Azad University, is gratefully acknowledged. The authors thank Dr. Ljungberg for the English editing.

References

- J. Tang, N. Lian, X. He, G. Zhang, *J. Mol. Struct.* **889**, 408–414 (2008)
- K. Tang, Y.M. Qin, A.H. Lin, X. Hu, G.L. Zou, *J. Pharm. Biomed. Anal.* **39**, 404–410 (2005)
- Y. Li, W. He, H. Liu, X. Yao, Z. Hu, *J. Mol. Struct.* **831**, 144–150 (2007)
- C.N. N'Soukpoe-Kossi, R. Sedaghat-Herati, C. Ragi, S. Hotchandani, H.A. Tajmir-Riahi, *Int. J. Biol. Macromol.* **40**, 484–490 (2007)
- F. Ding, W. Liu, Y. Li, L. Zhang, Y. Sun, *J. Lumin.* **130**, 2013–2021 (2010)
- M.A. Cheema, P. Taboada, S. Barbosa, J. Juárez, M. Gutiérrez-Pichel, M. Siddiq, V. Mosquera, *J. Chem. Thermodyn.* **41**, 439–447 (2009)
- D.C. Carter, J.X. Ho, *Adv. Protein Chem.* **45**, 153–203 (1994)
- A. Zarghi, S. Foroutan, A. Shafaati, A. Khoddam, *II Farmaco* **60**, 789–792 (2005)
- R. Tissier, S. Perrot, B. Enriquez, *J. Vet. Cardiol.* **7**, 53–58 (2005)
- J. Yoshida, T. Ishibashi, M. Nishio, *Eur. J. Pharmacol.* **472**, 23–31 (2003)
- B.E. Benson, D.A. Spyker, W.G. Troutman, W.A. Watson, L.N. Bakhireva, *J. Emerg. Med.* **39**, 186–193 (2010)
- A. Kapor, V. Nikolić, L. Nikolić, M. Stanković, M. Cakić, L. Stanojević, D. Ilić, *Open Chem.* **8**, 834–841 (2010)
- G. Zhang, Q. Que, J. Pan, J. Guo, *J. Mol. Struct.* **881**, 132–138 (2008)
- M.R. Housaindokht, Z. Rouhbakhsh Zaeri, M. Bahrololoom, J. Chamani, M.R. Bozorgmehr, *Spectrochim. Part A Mol. Biomol. Spectrosc.* **85**, 79–84 (2012)
- J. Równicka-Zubik, A. Sułkowska, J. Pożycka, K. Gaździcka, B. Bojko, M. Maciążek-Jurczyk, W. Sułkowski, *J. Mol. Struct.* **924**, 371–377 (2009)
- S. Patil, A. Sandberg, E. Heckert, W. Self, S. Seal, *Biomaterials* **28**, 4600–4607 (2007)
- G. Prieto, J. Sabín, J.M. Ruso, A. González-Pérez, F. Sarmiento, *Colloids Surf. A* **249**, 51–55 (2004)
- S.M. Darwish, S.E. AbuSharkh, M.M. AbuTeir, S.A. Makharza, M.M. Abu-hadid, *J. Mol. Struct.* **963**, 122–129 (2010)
- F. Ding, W. Liu, N. Li, L. Zhang, Y. Sun, *J. Mol. Struct.* **975**, 256–264 (2010)
- Y.-L. Wei, J.-Q. Li, C. Dong, S.-M. Shuang, D.-S. Liu, C.W. Huie, *Talanta* **70**, 377–382 (2006)
- F. Ding, J. Huang, J. Lin, Z. Li, F. Liu, Z. Jiang, Y. Sun, *Dyes Pigm.* **82**, 65–70 (2009)
- F. Ding, W. Liu, X. Zhang, L.-J. Wu, L. Zhang, Y. Sun, *Spectrochim. Acta Part A Mol. Biomol. Spectrosc.* **75**, 1088–1094 (2010)
- Y. Ni, S. Wang, S. Kokot, *Anal. Chim. Acta* **663**, 139–146 (2010)
- J.R. Lakowicz, G. Weber, *Biochemistry* **12**, 4161–4170 (1973)
- X. Yu, R. Liu, D. Ji, J. Xie, F. Yang, X. Li, H. Huang, P. Yi, *Spectrochim. Acta Part A Mol. Biomol. Spectrosc.* **77**, 213–218 (2010)
- I. Matei, M. Hillebrand, *J. Pharm. Biomed. Anal.* **51**, 768–773 (2010)
- D. Li, J. Zhu, J. Jin, X. Yao, *J. Mol. Struct.* **846**, 34–41 (2007)
- J. Tang, F. Luan, X. Chen, *Bioorg. Med. Chem.* **14**, 3210–3217 (2006)
- A. Sułkowska, M. Maciążek-Jurczyk, B. Bojko, J. Równicka, I. Zubik-Skupień, E. Temba, D. Pentak, W. Sułkowski, *J. Mol. Struct.* **881**, 97–106 (2008)
- K. Vuignier, J. Schappler, J.-L. Veuthey, P.-A. Carrupt, S. Martel, *J. Pharm. Biomed. Anal.* **53**, 1288–1297 (2010)
- J.-L. Yuan, H. Liu, X. Kang, Z. Lv, G.-L. Zou, *J. Mol. Struct.* **891**, 333–339 (2008)
- F. Ding, B.-Y. Han, W. Liu, L. Zhang, Y. Sun, *J. Fluoresc.* **20**, 753–762 (2010)
- D. Patra, T.H. Ghaddar, *Talanta* **77**, 1549–1554 (2009)

34. A. Mozo-Villarias, J. Biochem. Biophys. Methods **50**, 163–178 (2002)
35. V. Kumar, V.K. Sharma, D.S. Kalonia, Int. J. Pharm. **294**, 193–199 (2005)
36. Y. Zhang, J.-H. Li, Y.-S. Ge, X.-R. Liu, F.-L. Jiang, Y. Liu, J. Fluoresc. **21**, 475–485 (2011)
37. Y. Yue, X. Chen, J. Qin, X. Yao, Dyes Pigm. **79**, 176–182 (2008)
38. J.-L. Yuan, Z.-G. Liu, Z. Hu, G.-L. Zou, J. Photochem. Photobiol. A **191**, 104–113 (2007)
39. S.N. Khan, B. Islam, R. Yennamalli, A. Sultan, N. Subbarao, A.U. Khan, Eur. J. Pharm. Sci. **35**, 371–382 (2008)
40. Y. Ni, D. Lin, S. Kokot, Anal. Biochem. **352**, 231–242 (2006)
41. L.-Y. Wang, Y.-Y. Zhou, L. Wang, C.-Q. Zhu, Y.-X. Li, F. Gao, Anal. Chim. Acta **466**, 87–92 (2002)
42. X.-C. Shen, X.-Y. Liou, L.-P. Ye, H. Liang, Z.-Y. Wang, J. Colloid Interface Sci. **311**, 400–406 (2007)
43. H. Yang, Y. Wang, Y. Wang, J. Li, X. Xiao, X. Tan, Spectrochim. Acta Part A Mol. Biomol. Spectrosc. **71**, 1290–1295 (2008)
44. L. Li, Z.S. Xu, Q. Pan, G.W. Song, J. Fluor. Chem. **130**, 567–572 (2009)
45. K. Cai, M. Frant, J. Bossert, G. Hildebrand, K. Liefeyth, K.D. Jandt, Colloids Surf. B **50**, 1–8 (2006)
46. A. Chakrabarty, A. Mallick, B. Haldar, P. Das, N. Chattopadhyay, Biomacromol **8**, 920–927 (2007)
47. A. Oliveira, M. Ferraz, F. Monteiro, S. Simoes, Acta Biomater. **5**, 2142–2151 (2009)
48. P. Atkins, J. De Paula, *Elements of Physical Chemistry* (Oxford University Press, USA, 2013)
49. L. He, X. Wang, B. Liu, J. Wang, Y. Sun, E. Gao, S. Xu, J. Lumin. **131**, 285–290 (2011)
50. Y. Xiang, F. Wu, Spectrochim. Acta Part A Mol. Biomol. Spectrosc. **77**, 430–436 (2010)
51. F. Ding, W. Liu, F. Liu, Z.-Y. Li, Y. Sun, J. Fluoresc. **19**, 783–791 (2009)
52. S.C. Rao, C. Rao, FEBS Lett. **337**, 269–273 (1994)
53. M.C. Tory, A.R. Merrill, Biochimica et Biophysica Acta (BBA)-Biomembranes **1564**, 435–448 (2002)
54. H. Raghuraman, A. Chattopadhyay, Biophys. J. **87**, 2419–2432 (2004)
55. A. Chattopadhyay, R. Rukmini, FEBS Lett. **335**, 341–344 (1993)
56. Q. Xiao, S. Huang, Y. Liu, F.-F. Tian, J.-C. Zhu, Journal of fluorescence **19**, 317–326 (2009)
57. B. Schuler, ChemPhysChem **6**, 1206–1220 (2005)
58. S. Laib, S. Seeger, J. Fluoresc. **14**, 187–191 (2004)
59. S.M. Kelly, T.J. Jess, N.C. Price, Biochimica et Biophysica Acta (BBA)-Proteins and Proteomics **1751**, 119–139 (2005)
60. S.Y. Tetin, F.G. Prendergast, S.Y. Venyaminov, Anal. Biochem. **321**, 183–187 (2003)
61. R. Banerjee, G. Basu, FEBS Lett. **523**, 152–156 (2002)
62. P. Bourassa, S. Dubeau, G.M. Maharvi, A.H. Fauq, T. Thomas, H. Tajmir-Riahi, Eur. J. Med. Chem. **46**, 4344–4353 (2011)
63. V. Reipa, M. Holden, M.P. Mayhew, V.L. Vilker, Biochem. Biophys. Acta. **1699**, 229–234 (2004)
64. W. An, Y. Jiao, C. Dong, C. Yang, Y. Inoue, S. Shuang, Dyes Pigm. **81**, 1–9 (2009)